

In presenting the dissertation as a partial fulfillment of the requirements for an advanced degree from the Georgia Institute of Technology, I agree that the Library of the Institute shall make it available for inspection and circulation in accordance with its regulations governing materials of this type. I agree that permission to copy from, or to publish from, this dissertation may be granted by the professor under whose direction it was written, or, in his absence, by the Dean of the Graduate Division when such copying or publication is solely for scholarly purposes and does not involve potential financial gain. It is understood that any copying from, or publication of, this dissertation which involves potential financial gain will not be allowed without written permission.

7/25/68

EMISSION OF MICROWAVE RADIATION

BY GASES

A THESIS

Presented to

The Faculty of the Graduate Division

by

Foch Tsai

In partial Fulfillment

of the Requirements for the Degree

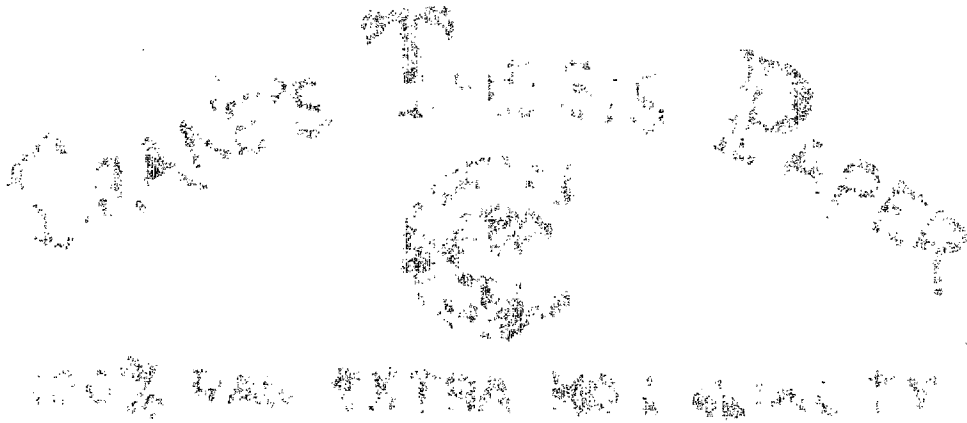
Doctor of Philosophy in the School of Physics

Georgia Institute of Technology

December, 1972

EMISSION OF MICROWAVE RADIATION

BY GASES



Approved:

Chairman

Date approved by Chairman: 29 Nov 1972

## ACKNOWLEDGMENTS

I wish to thank Dr. T. L. Weatherly and Dr. J. Q. Williams for their guidance, encouragement and invaluable help which made this work possible. Also I am much indebted to Dr. R. C. Johnson for his suggestions through our discussions. A special note of appreciation is due to my wife, Betty, whom I owe more than I can possibly express.

I acknowledge the financial help from Southern Fellowship Fund for the Faculty Fellowship during the summer of 1972. Sincere thanks are also due to Dr. Hugh M. Gloster, the president of Morehouse College, and to physics faculty members at Morehouse College for their encouragement and their willingness to help on many occasions.

## TABLE OF CONTENTS

	Page
ACKNOWLEDGEMENTS.....	ii
LIST OF TABLES.....	iv
LIST OF ILLUSTRATIONS.....	v
Chapter	
I. INTRODUCTION.....	1
II. THEORETICAL BACKGROUND.....	5
Adiabatic Rapid Passage of Nuclear Magnetic Resonance Microwave Adiabatic Rapid Passage Stark Sweep Method	
III. EXPERIMENTAL PROCEDURE.....	24
General Experimental Apparatus Data Collection Procedure	
IV. RESULTS OF INVESTIGATION.....	35
Observation of Microwave Emission under Different Conditions The Relation of Decay Rate and Other Physical Parameters The Relation Between Signal Amplitude and Other Physical Parameters The Emission Radiation Power	
V. CONCLUSIONS AND RECOMMENDATIONS.....	74
APPENDIX A.....	77
APPENDIX B.....	83
APPENDIX C.....	87
LITERATURE CITED.....	99
VITA.....	101

## LIST OF TABLES

Table		Page
1.	Pressure, Signal Amplitude and Time Constant of OCS $J = 2 \rightarrow 1$ .....	55
2.	Pressure, Signal Amplitude and Time Constant for $\text{NH}_3$ .....	59
3.	Pressure and Temperature Factor X.....	64
4.	OCS Data of Figure 26.....	88
5.	$\text{NH}_3$ Data of Figure 28.....	91
6.	Temperature Influence on Time Constant.....	95
7.	Signal Amplitude and Temperature Relation.....	97
8.	Signal Amplitude and Klystron Power Relation.....	98

LIST OF ILLUSTRATIONS

Figure	Page
1. Diagram of the Effective Field and Magnetic Moment in the Rotating Frame.....	6
2. Curves of the Probabilities $P(\pm\frac{1}{2})$ at Resonance.....	8
3. Successive Positions of $H_e$ as $\omega$ is Swept through $H_0$ .....	8
4. The Variation of Ground and Excited State Populations with Time.....	13
5. The Klystron Frequency Sweep through Resonance and Interchange of State Populations in Microwave Adiabatic Rapid Passage.....	14
6. Ground and Excited State Populations during Adiabatic Passage, Ideal Case.....	16
7. Ground and Excited State Populations during Adiabatic Passage, Larger Power.....	17
8. Ground and Excited State Populations during Adiabatic Passage, Smaller Power.....	18
9. Ground and Excited State Populations during Adiabatic Passage, Faster Sweep Rate.....	19
10. Ground and Excited State Populations during Adiabatic Passage, Slower Sweep Rate.....	20
11. Relation between Stark Field, Frequency of Stark Components and Frequency of Klystron.....	22
12. Block Diagram of Spectrograph.....	25
13. Relation of the Frequencies Used in the Frequency Lock-in System.....	29
14. RC-circuit Used for Measuring the Time Constant.....	31
15. Relation between Time Constant and Dial Reading...	32

## LIST OF ILLUSTRATIONS (Continued)

Figure	Page
16. Matching of the Exponential Curve with Different Peaks.....	34
17. Observation of Microwave Emission under Raising and Falling Stark Voltage.....	36
18. Observation of Microwave Emission under Different Number of Stark Components.....	38
19. Observation of Microwave Emission under Different Sweep Rates.....	39
20. Observation of Microwave Emission under Two Opposite Extremes of Klystron Power.....	40
21. Observation of Microwave Emission under Different Stark Voltages.....	42
22. Observation of Microwave Emission under Different Pressures.....	46
23. Observation of Microwave Emission under Different Temperatures.....	49
24. Observation of Microwave Emission under Different Samples at Low Pressures.....	50
25. Reciprocal Time Constants versus Pressure, OCS $J = 2 \rightarrow 1$ , $V = 0$ .....	54
26. Results of Six Sets of Measurements of Time Constant and Pressure of OCS $J = 2 \rightarrow 1$ , $V = 0$ .....	56
27. Reciprocal Time Constants versus Pressure, $\text{NH}_3$ (3,3).....	58
28. Results of Five Sets of Measurements of Time Constant and Pressure of $\text{NH}_3$ (3,3).....	60
29. Relationship of Time Constant and Temperature, $\text{NH}_3$ (3,3).....	63
30. Signal Amplitude and Pressure Relation.....	67

## LIST OF ILLUSTRATIONS (Continued)

Figure		Page
31.	Signal Amplitude and Temperature Relation.....	69
32.	Signal Amplitude and Klystron Power Relation.....	70
33.	Block Diagram of Apparatus Used for the Radiation Power Measurement.....	72

UNIVERSITY OF MICHIGAN  
THESIS  
MICHIGAN STATE UNIVERSITY

## CHAPTER I

### INTRODUCTION

Recently one of the interests of the microwave group in the School of Physics at Georgia Institute of Technology has been the study of the emission of microwave radiation by gases. When a molecule with ground state wave function is subject to resonance radiation, its wave function becomes a mixture of ground and excited state wave functions. Its dipole moment will then oscillate at the resonant frequency producing radiation which is out of phase with the inducing radiation. If the inducing radiation is of short duration, then after it terminates the molecule will continue to radiate until it returns to the ground state or until it has a collision.

Romer and Dicke (1) were the first to observe this type of radiation from a gas. In 1955 they announced a method for exciting gases to states from which they emit coherent spontaneous radiation in the microwave frequency region. The excitation was produced by the application of short pulses of microwave power. The power subsequently radiated by the gas was calculated for several cases and the experimental methods used to detect the radiation are des-

cribed in their paper. In 1967, Hill, Kaplan, Hermann and Ichiki (2) reported the emission of microwave radiation from OCS excited by short microwave pulses. They observed a coherent ringing after termination of the incident pulses, and the decay envelope of this radiation provided direct information on collision rates and other relaxation processes.

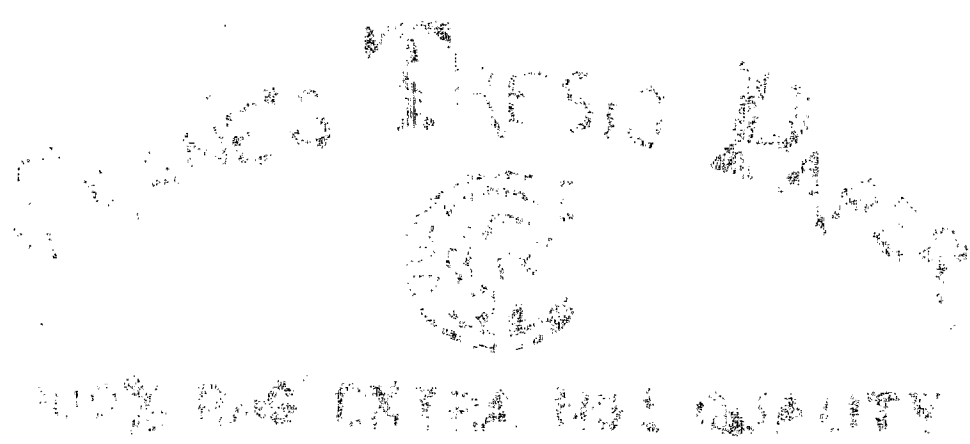
The microwave group in the School of Physics at Georgia Institute of Technology has found a different method for exciting the gas which is related to the adiabatic rapid passage phenomenon in nuclear magnetic resonance. The phenomenon is usually explained on the basis of a classical model of magnetism, but it has been shown in this work to be applicable to systems for which no classical model is possible. Excitation of the gas is accomplished by sweeping the frequency of the applied radiation through the resonance frequency of the gas rather than subjecting the gas to a very short pulse of radiation. If a pulse is used the microwave power and duration of pulse must be very carefully adjusted, but if the sweep method is used neither the power nor sweep rate are critical adjustments. The sweep method is more than just a way of obtaining a short pulse. In the actual application of the sweep method in the laboratory the frequency of the incident radiation is held fixed and the resonance frequency of the gas is swept by use of the Stark effect. Having the incident radiation constant in amplitude and fixed in frequency is a very great advantage experimentally. If

the klystron frequency is varied the klystron power at the crystal detector changes because of the nonuniform power output of the klystron and reflections in the Stark cell. These power variations have a much larger effect on the detected signal than the molecular radiation. On the other hand if the klystron radiation has constant amplitude and frequency then one can be sure that any variation of the beat signal is produced by the molecular radiation.

The primary concern of this investigation has been to show that the adiabatic rapid passage technique can be used to excite gas molecules making possible an observation of their microwave emission spectra. The decay rate of the emitted radiation after excitation has proven to be of particular interest, and its measurement has yielded some surprises.

A theoretical discussion of the quantum mechanical treatment of this type of emission radiation and its comparison with the adiabatic rapid passage method of nuclear magnetic resonance will be found in Chapter II. Discussion of the experimental method and data collection are found in Chapter III. The results of this investigation can be divided into two main categories, namely, the observation of emission radiation under different physical conditions, such as, different number of Stark components, different Stark voltage and different sweep rate, etc., and the relation of decay rate to pressure, temperature and power. These

results are discussed in Chapter IV. Finally a report about conclusions and recommendations is given in Chapter V.



## CHAPTER II

## THEORETICAL BACKGROUND

Adiabatic Rapid Passage of Nuclear Magnetic Resonance

Consider a top with total angular momentum  $\vec{J}\hbar$  which carries a negative electric charge and is subjected to a constant magnetic field  $\vec{H}_0$ . The well known result for this top is that the magnetic moment vector,  $\vec{\mu} = -g\hbar\vec{J}$ , precesses at a constant rate at a fixed angle with  $\vec{H}_0$  and at Larmor frequency  $\vec{\omega}_0 = \gamma\vec{H}_0$ , where  $g$  is the spectroscopic splitting factor and  $\gamma$  is the magnetogyric ratio or gyromagnetic ratio.

If, instead of applying just a constant magnetic field  $\vec{H}_0$ , one adds a rotating component  $\vec{H}_1$  at right angles to  $\vec{H}_0$  then the total field can be expressed

$$\vec{H} = \hat{i} H_1 \cos \omega t + \hat{j} H_1 \sin \omega t + \hat{k} H_0. \quad (1)$$

By viewing from a coordinate system rotating at the same frequency as  $\vec{H}_1$ , namely  $\omega$ , the effective field will be  $\vec{H}_e = \vec{H} - \vec{\omega}/\gamma$  as indicated on Figure 1. From the classical mechanics of tops it can be shown that the magnetic moment  $\mu$  will, in the second rotating system, rotate at  $\vec{\omega}' = \gamma\vec{H}_e$  about the direction of  $\vec{H}_e$ . Since only the z-component of  $\vec{\mu}$  determines the energy, only  $\cos \alpha$  is needed. By straight-

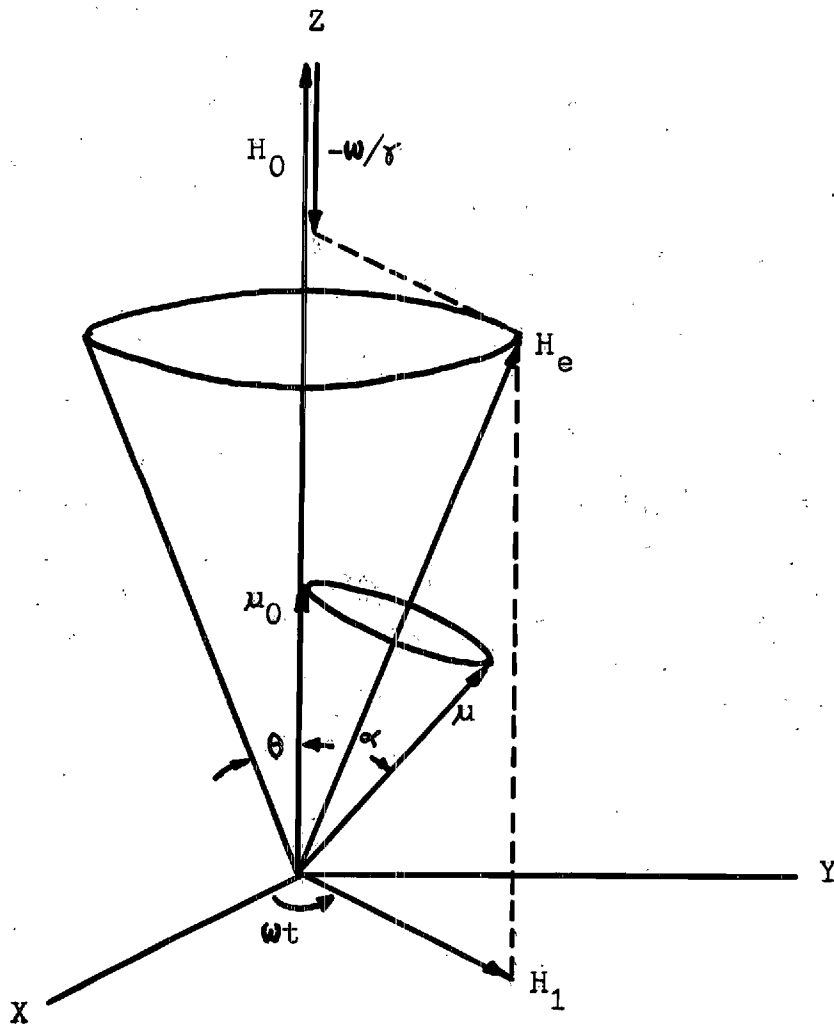


Figure 1. Diagram of the Effective Field and Magnetic Moment in the Rotating Frame.

forward trigonometry one can show from Figure 1 that

$$\cos \alpha = 1 - 2 \sin^2 \theta \sin^2 \left( \frac{1}{2} \omega' t \right). \quad (2)$$

If one supposes the magnetic moment  $\vec{\mu}$  to arise from a particle of spin  $J=S=\frac{1}{2}$ , then  $\cos \alpha$  can be used to give the probability  $P(-\frac{1}{2})$  that  $\langle S_z \rangle = -\frac{1}{2}$  where initially at  $t=0$   $\langle S_z \rangle = +\frac{1}{2}$ . Since the classical z-component is  $\frac{1}{2} \cos \alpha$  one has

$$\frac{1}{2} \cos \alpha = \frac{1}{2} P(+\frac{1}{2}) - \frac{1}{2} P(-\frac{1}{2}) \quad (3)$$

and  $P(+\frac{1}{2}) + P(-\frac{1}{2}) = 1$ . Eliminating  $P(+\frac{1}{2})$  one gets

$$P(-\frac{1}{2}) = \frac{1}{2} (1 - \cos \alpha) = \sin^2 \theta \sin^2 \left( \frac{1}{2} \omega' t \right) \quad (4)$$

From Figure 1 it can be seen that  $\sin \theta = H_1 / H_e$ , and since  $\omega' = \gamma H_e$ , one obtains

$$\sin \frac{1}{2} \omega' t = \sin \frac{1}{2} \gamma H_e t = \sin \frac{1}{2} \gamma t \left[ H_1^2 + (H_0 - \omega/\gamma)^2 \right]^{\frac{1}{2}} \quad (5)$$

Finally, one obtains

$$P(-\frac{1}{2}) = \frac{H_1^2}{H_1^2 + (H_0 - \omega/\gamma)^2} \sin^2 \left\{ \frac{1}{2} t \left[ \gamma^2 H_1^2 + (\gamma H_0 - \omega)^2 \right]^{\frac{1}{2}} \right\} \quad (6)$$

Consider the special case when  $\vec{\omega} = \vec{H}_0 \gamma = \vec{\omega}_0$ . From Figure 1 it can be seen that  $\theta = \pi/2$  and  $\vec{H}_e = \vec{H}_1$ . Equation (6) becomes

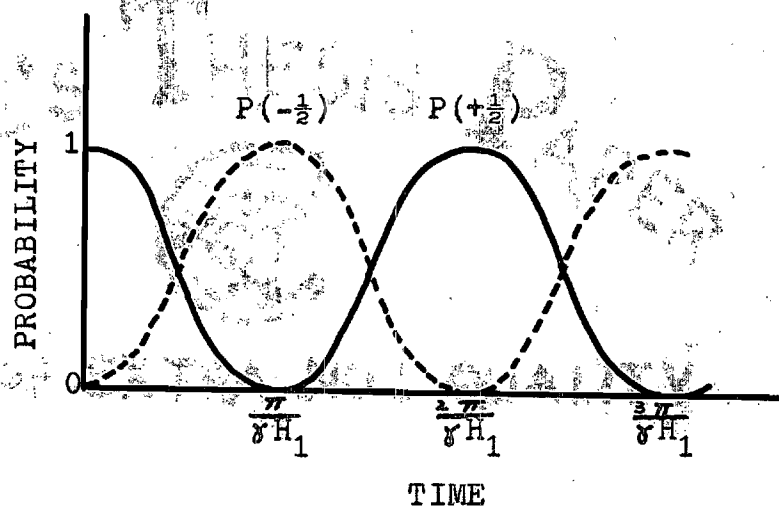


Figure 2. Curves of the Probabilities  $P(-\frac{1}{2})$  and  $P(+\frac{1}{2})$  at Resonance.

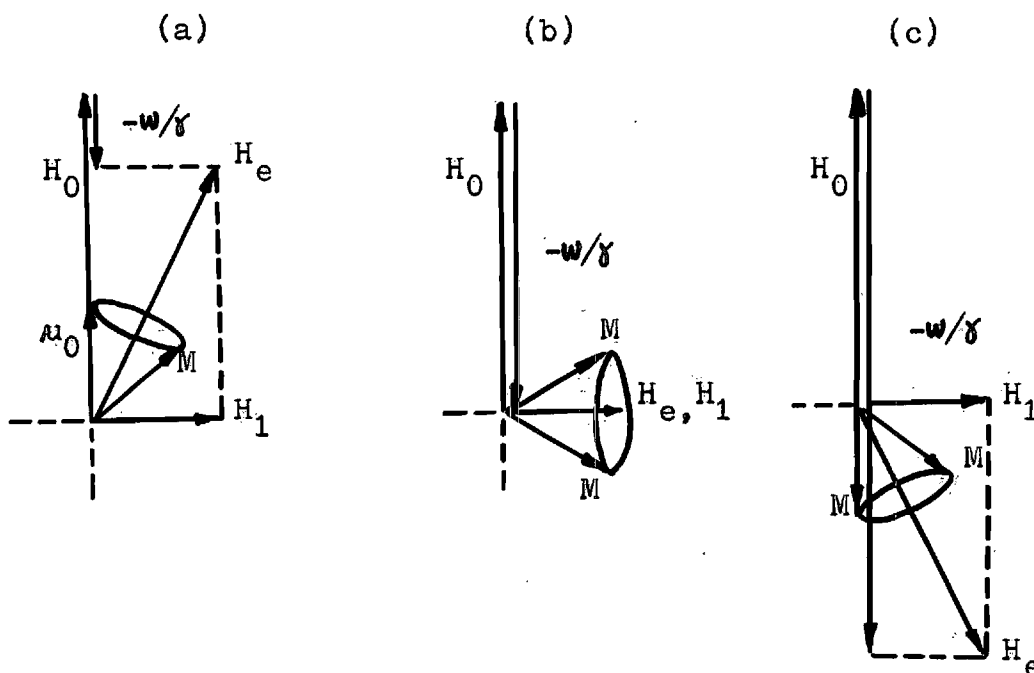


Figure 3. Successive Positions of  $\vec{H}_e$  and  $\vec{M}$  as  $\omega$  is Swept through  $\gamma H_0$ .

$$P(-\frac{1}{2}) = \sin^2 (\frac{1}{2}\gamma H_1 t). \quad (7)$$

The magnetic moment oscillates between the +z and -z direction and the initial probabilities  $P(+\frac{1}{2})$  and  $P(-\frac{1}{2})$  have been interchanged at the times when  $t = (2n+1)\pi/\gamma H_1$  where  $n = 0, 1, 2, 3, \dots$  as shown on Figure 2. This is the case called magnetic resonance. It occurs when  $\vec{\omega}$  is equal to  $\vec{\omega}_0$ , the Larmor precession frequency of an isolated moment.

The above discussion is based upon a single particle model, but the results can be used to predict the behavior of the total magnetization  $\vec{M}$  which is just the vector sum of the  $\vec{\mu}_i$ 's over a unit volume. Generally, the magnetization  $\vec{M}$  tends exponentially toward its thermal equilibrium value  $\vec{M}_0$  if no external interactions influence it. If somehow a nonequilibrium  $\vec{M}$  has been achieved, say by turning the rotating field  $\vec{H}_1$  on and off briefly, then  $\vec{M}$  will tend to precess at  $\omega_0$  except for the effects of relaxation. Consider the case when a slow sweep of the magnitude of  $\vec{\omega}$  from  $\omega < \omega_0$  through  $\omega = \omega_0$  to  $\omega > \omega_0$  occurs. Figure 3 pictures the successive positions of  $\vec{H}_e$  in the plane of  $\vec{H}_0$  and  $\vec{H}_1$  during the sweep process. (Recall that this plane is precessing rapidly around  $\vec{H}_0$  relative to the laboratory reference frame.) Initially, as shown on part (a),  $\vec{M}$  is pointing approximately along  $\vec{H}_0$  and precessing about  $\vec{H}_e$ . As  $\omega$  increases the vector  $\vec{H}_e$  approaches the direction  $\vec{H}_1$  and  $\vec{M}$  precesses around a cone

with  $\vec{H}_e$  as axis. When  $\omega$  reaches  $\omega_0$  as part (b) shows,  $\vec{M}$  moves around a circle in a plane perpendicular to  $\vec{H}_1$ . As the value of  $\omega$  becomes greater than  $\omega_0$  as shown on part (c),  $\vec{M}$  will start precessing into the direction which is anti-parallel to  $\vec{H}_0$ . Therefore during the sweep of  $\omega$  through  $\omega_0$ ,  $\vec{M}$  completely flips from the  $+\vec{H}_0$  to  $-\vec{H}_0$  direction. A coil placed around the sample and having its axis in the equatorial plane will experience a varying flux linkage and hence an emf which reaches a maximum with  $\vec{M}$  in the equatorial plane. Two conditions need to be considered. The first is how slowly must  $\vec{H}_e$  be turned (or how slowly must  $\omega$  be swept) so that  $\vec{M}$  will follow. The second is how fast  $\vec{H}_e$  must change in a short time so that  $\vec{M}$  will not relax back to  $\vec{M}_0$  before the process of reversing  $\vec{H}_e$  has been completed. Bloch (3) applied the relaxation theory and introduced the time constant of exponential decay  $T$  to give the following conditions

$$\frac{1}{T} \ll \frac{1}{H_1} \left| \frac{d}{dt} (H_0 - \frac{\omega}{\gamma}) \right| \gg \gamma H_1. \quad (8)$$

From these two conditions this method is named the "adiabatic rapid passage method".

#### Microwave Adiabatic Rapid Passage

The microwave adiabatic rapid passage method is similar to the corresponding nuclear magnetic resonance method just discussed. However this method of excitation

can be used to excite systems where no classical model is available. Again this method can be divided into two parts, namely, pulsing at fixed frequency and sweeping through the resonance.

Consider a two level system in which  $\Psi_g$  and  $\Psi_e$  are the time dependent eigenfunctions of ground and excited states respectively. Suppose that initially the system is in the ground state and that at  $t = 0$  it is subjected to radiation at the resonance frequency  $\nu_R$  which causes a transition to the excited state. The wavefunction at a later time can be expressed as

$$\Psi(t) = a_g(t) \Psi_g(t) + a_e(t) \Psi_e(t) \quad (9)$$

where initially  $a_g(0) = 1$  and  $a_e(0) = 0$ . The time rate of change of the coefficients are given by time dependent perturbation theory as

$$\begin{aligned} \dot{a}_e(t) &= (-1/\hbar) a_g(t) \int \Psi_e^*(t) H \Psi_g(t) d\tau \\ \dot{a}_g(t) &= (-1/\hbar) a_e(t) \int \Psi_g^*(t) H \Psi_e(t) d\tau \end{aligned} \quad (10)$$

where  $H$  is the Hamiltonian for the interaction between the radiation and the system. For a microwave radiation field polarized in the  $z$ -direction,  $H$  is given by

$$H = - \vec{\mu} \cdot \vec{E} = - \mu_z E_z, \quad (11)$$

where  $\mu_z$  is the z-component of the molecular electric dipole moment and  $E_z$  is the intensity of the microwave electric field. A solution of equations (10), as shown in detail in Appendix A, gives for the probability of the system being in the excited state  $a_e^* a_e = \sin^2 ct$  and for the ground state  $a_g^* a_g = \cos^2 ct$  where  $c$  in the case of electric dipole interaction is equal to the matrix element of the dipole moment operator for the transition times the microwave field intensity divided by  $2\hbar$ . The plot of the probabilities versus the time are shown in Figure 4. From that plot it can be seen that initially the probability of the system being in the ground state,  $a_g^* a_g$ , has the value 1, and the probability of it being in the excited state  $a_e^* a_e$  is zero. If the microwave radiation with frequency fixed at resonance is cut off at time  $t_1$ , as shown on Figure 4, the system would have gone from ground state to excited state. If there are many systems, some initially in the ground state and some in the excited state, then these populations would be reversed by the pulse of radiation. In order to obtain this reversal the intensity and duration of the pulse would have to be very carefully adjusted.

The population reversal can also be achieved by a method similar to the adiabatic rapid passage method of

nuclear magnetic resonance. That is, one can start with the radiation frequency lower than the resonance frequency and then increase it in order to sweep through the resonance frequency as shown in Figure 5.

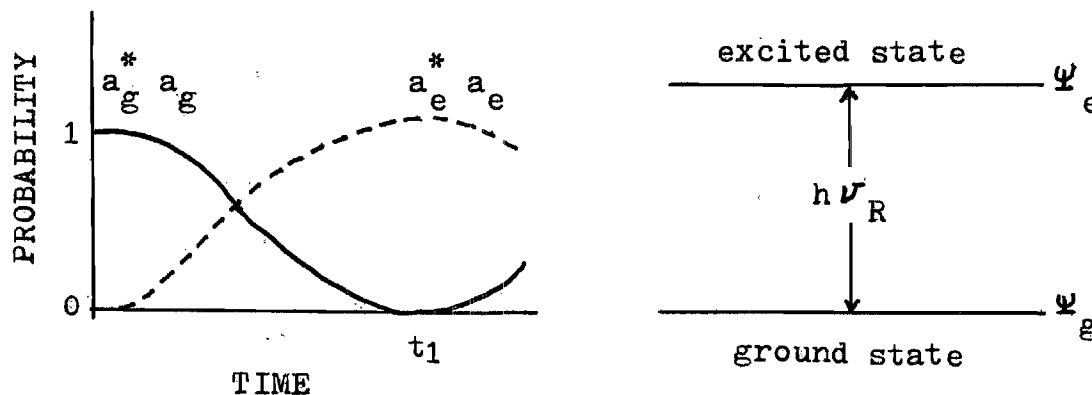


Figure 4. The Variation of Ground and Excited State Populations With Time.

Starting from the initial condition, the probability for the molecule being in the ground state  $a_g^*$   $a_g$  is one and the probability of it being in the excited state  $a_e^*$   $a_e$  is zero. The probabilities at later times are found by solving equations (10). As the sweep occurs these probabilities undergo some small oscillations then interchange values as the radiation frequency passes through the resonance frequency. The rate of sweep and the radiation field intensity are not critical in this case so long as the sweep is fast enough that the relaxation processes do not prevent the reversal.

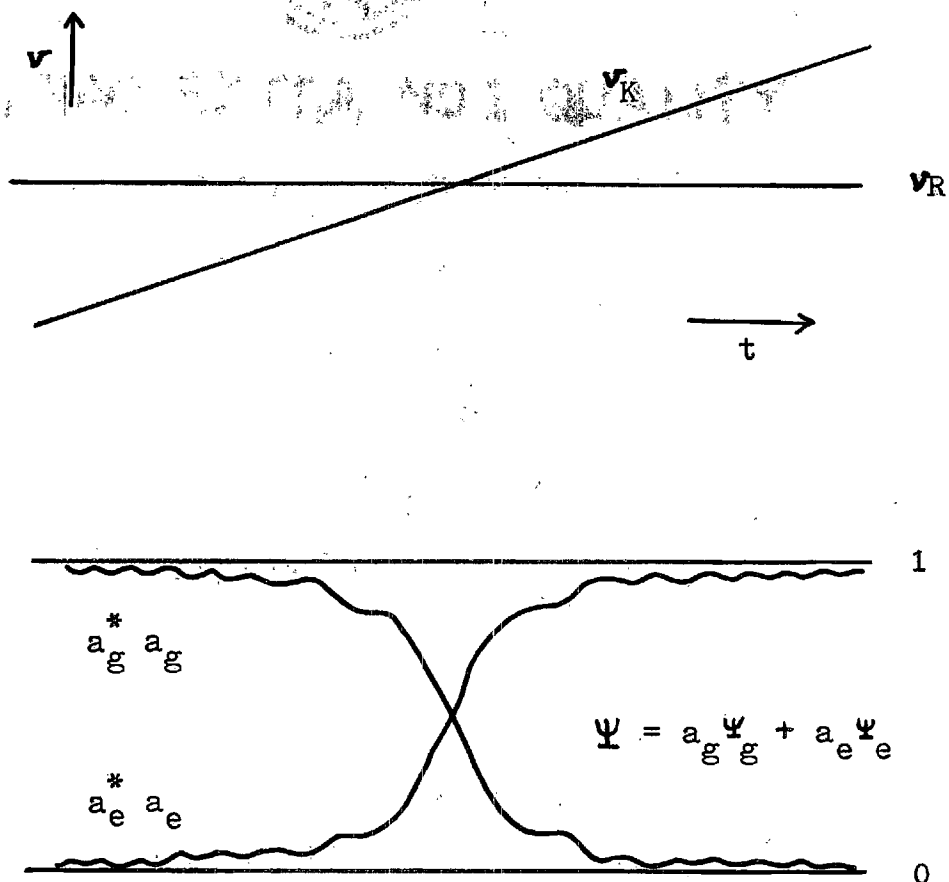


Figure 5. The Klystron Frequency Sweep through Resonance and Interchange of State Populations in Microwave Adiabatic Rapid Passage.

For the purpose of making an accurate calculation of the populations during this reversal process a computer program was written as described in Appendix B. The results of this computer calculation are plotted in Figures 6 to 10. In these figures, the horizontal coordinate is the time and each unit represents 0.4 nanosecond. The vertical coordinates, running from 0 to 1, represent the probabilities of the molecules being in ground or excited states. The solid curves show the change of these probabilities with time when initially the molecules were concentrated in the ground state, while the dashed curves show the probabilities when the molecules were initially in the excited state.

Figure 6, shows an ideal complete reversal case with small oscillations, and Figure 7 and 10 show the effects of varying the conditions required for the ideal case. In Figure 6,  $c = E_x^0 \mu_{xmn} / 2\hbar$  is set at the optimum value,  $40 \times 10^6$  rad/sec.  $C$  increases with increasing microwave power. The number of intervals  $N$  into which the sweep is divided for the calculations is 10,000 in all cases. The time for half a sweep,  $L$ , is set at 0.4 microsecond in Figure 6. That is the full sweep requires 0.8 microseconds. The sweep rate  $K$  is  $10^{15}$  rad/sec. Figure 7 shows the effect of increasing the power two and one half times. The oscillations become larger and faster but the reversal process is still complete. Notice from the figure some values of the probabilities are more than one indicating that the wave function

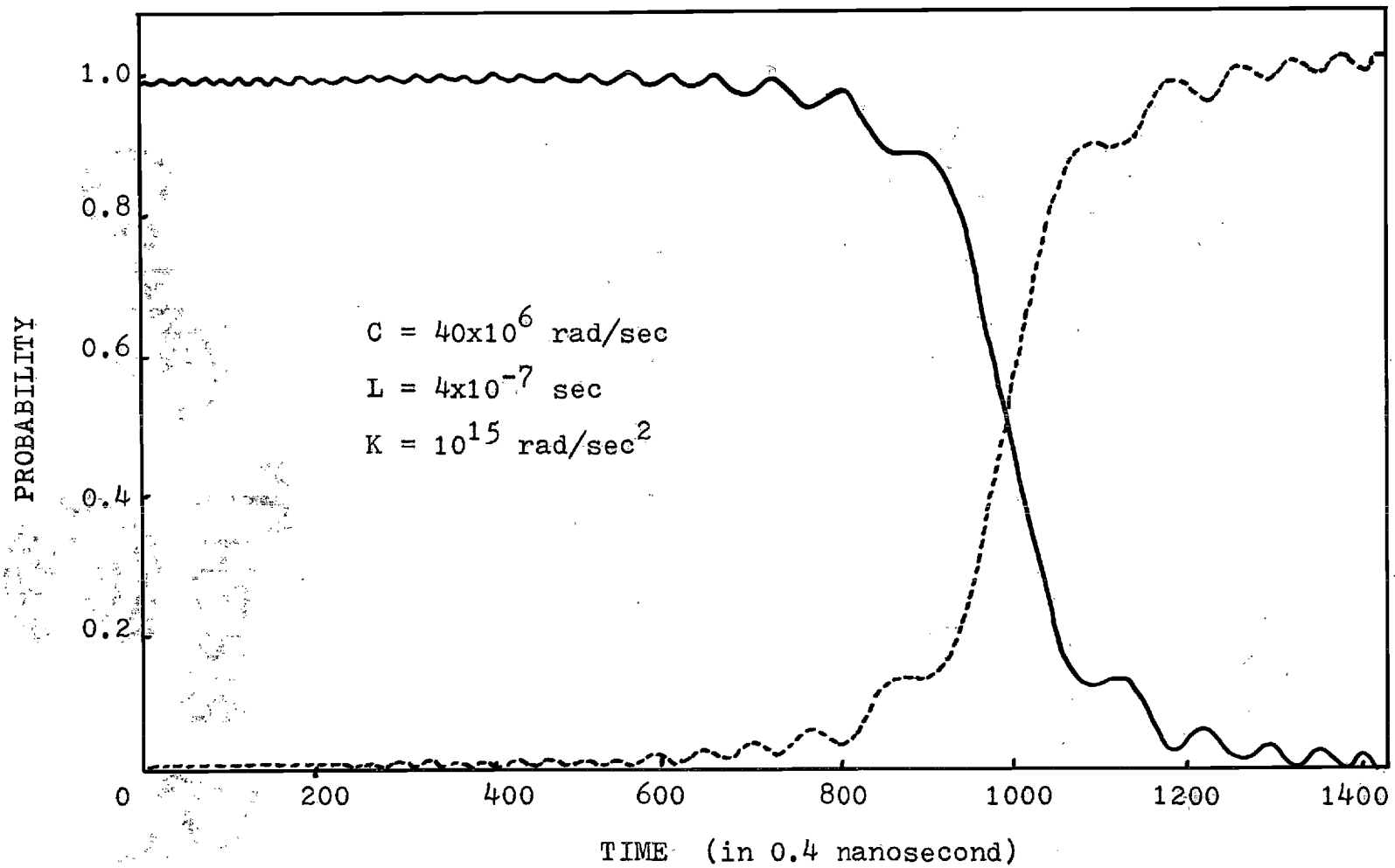


Figure 6. Ground and Excited State Populations during Adiabatic Rapid Passage, Ideal Case.

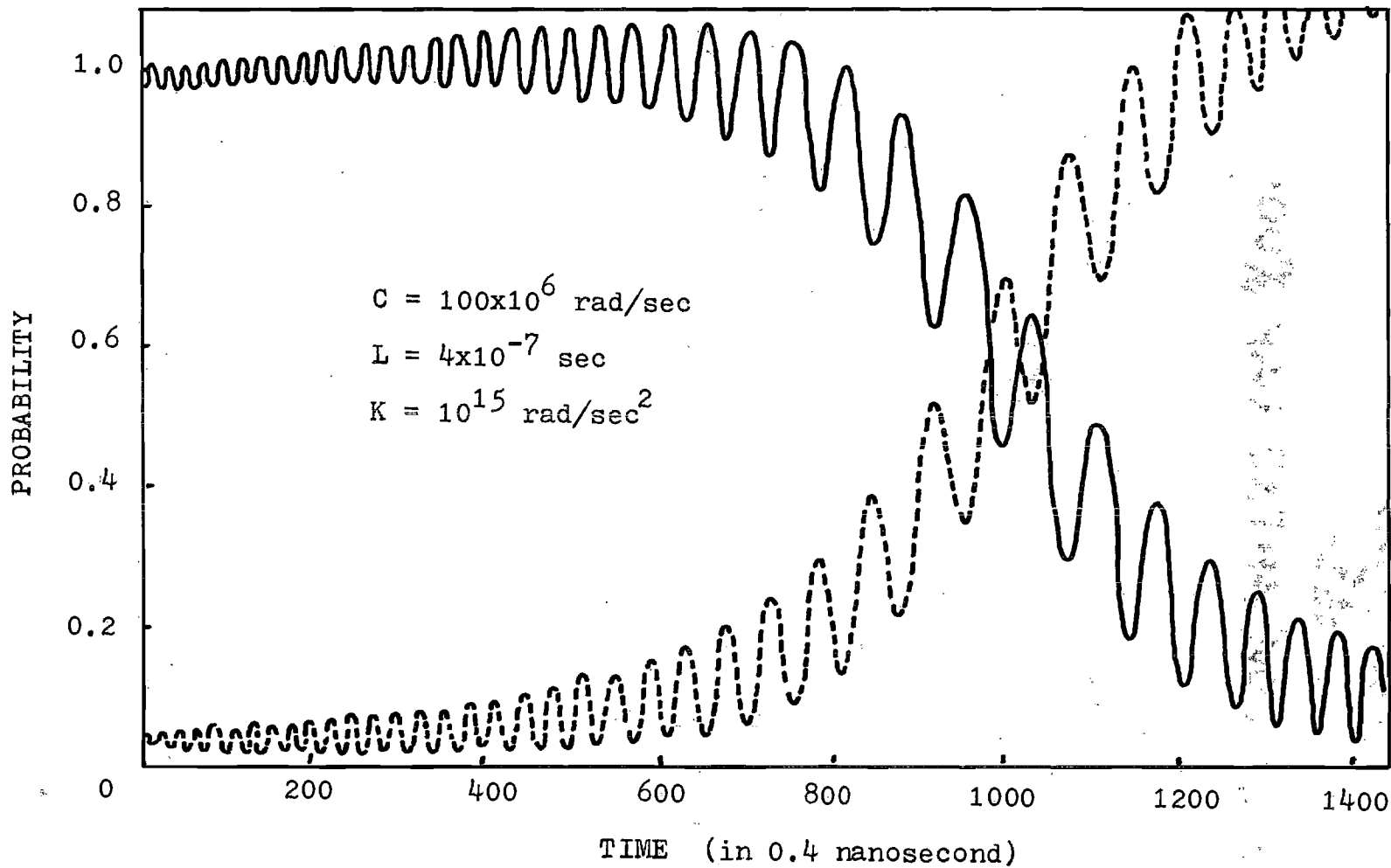


Figure 7. Ground and Excited State Populations during Adiabatic Rapid Passage, Larger Power.

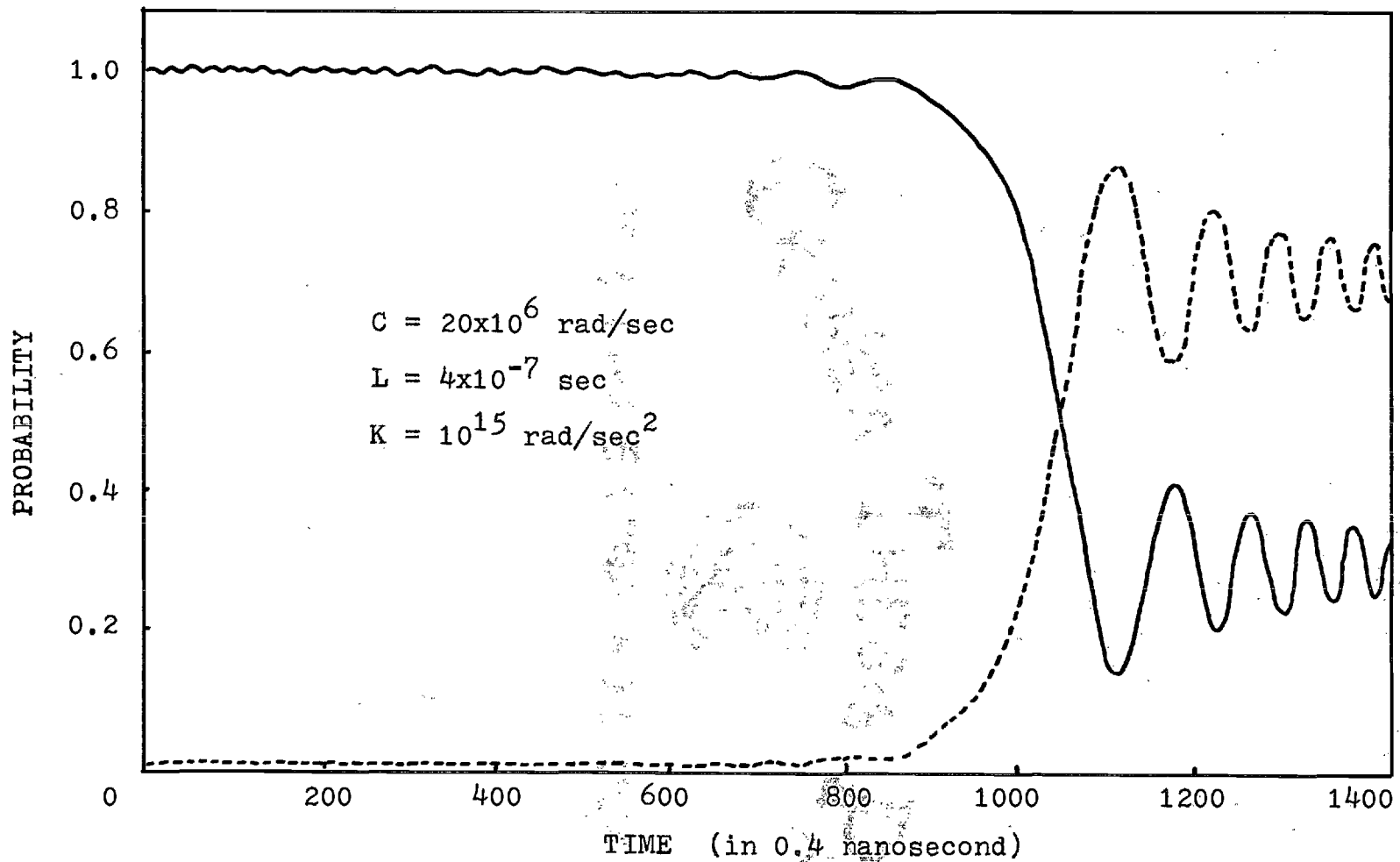


Figure 8. Ground and Excited State Populations during Adiabatic Rapid Passage, Smaller Power.

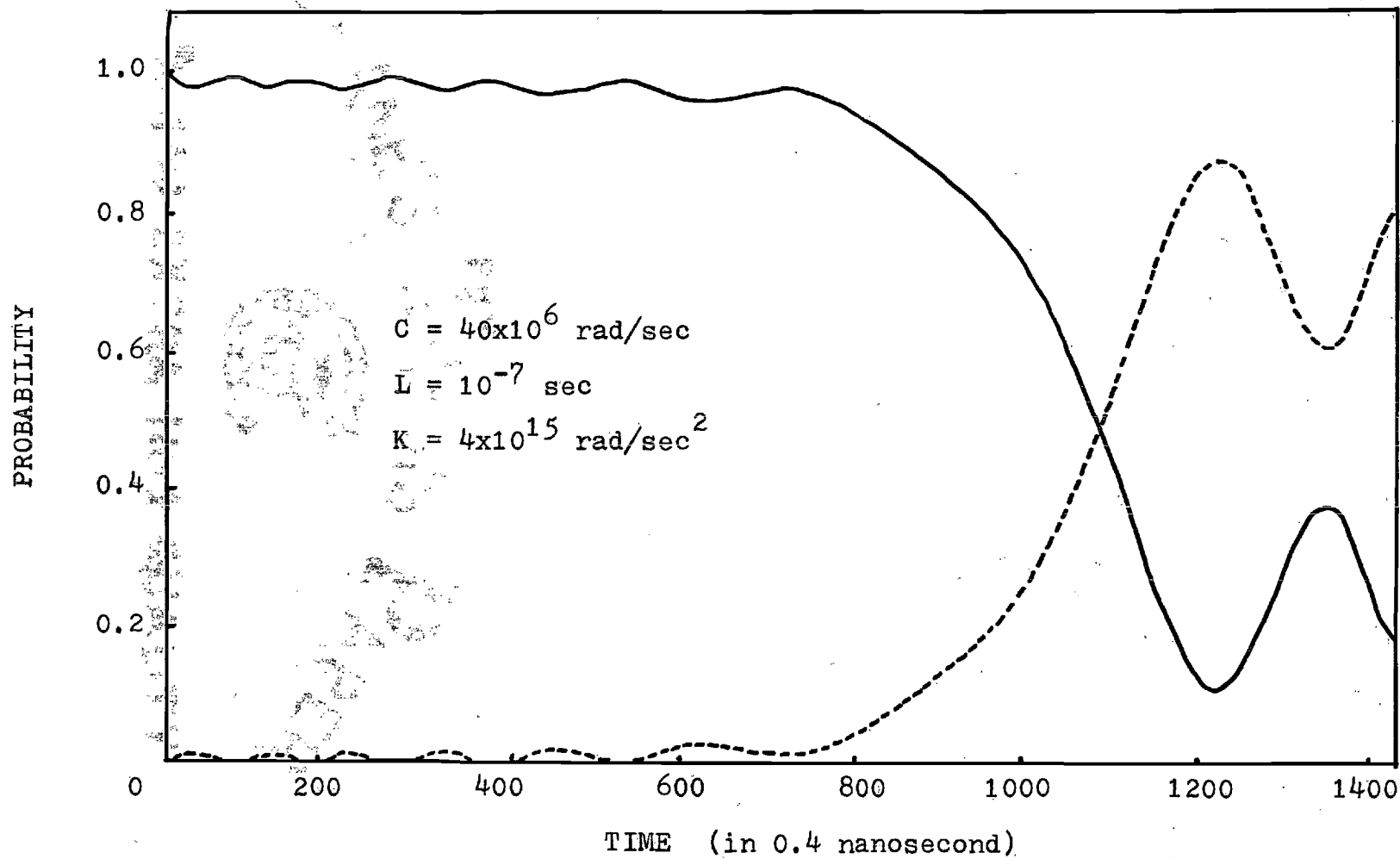


Figure 9. Ground and Excited State Populations during Adiabatic Rapid Passage, Faster Sweep Rate.

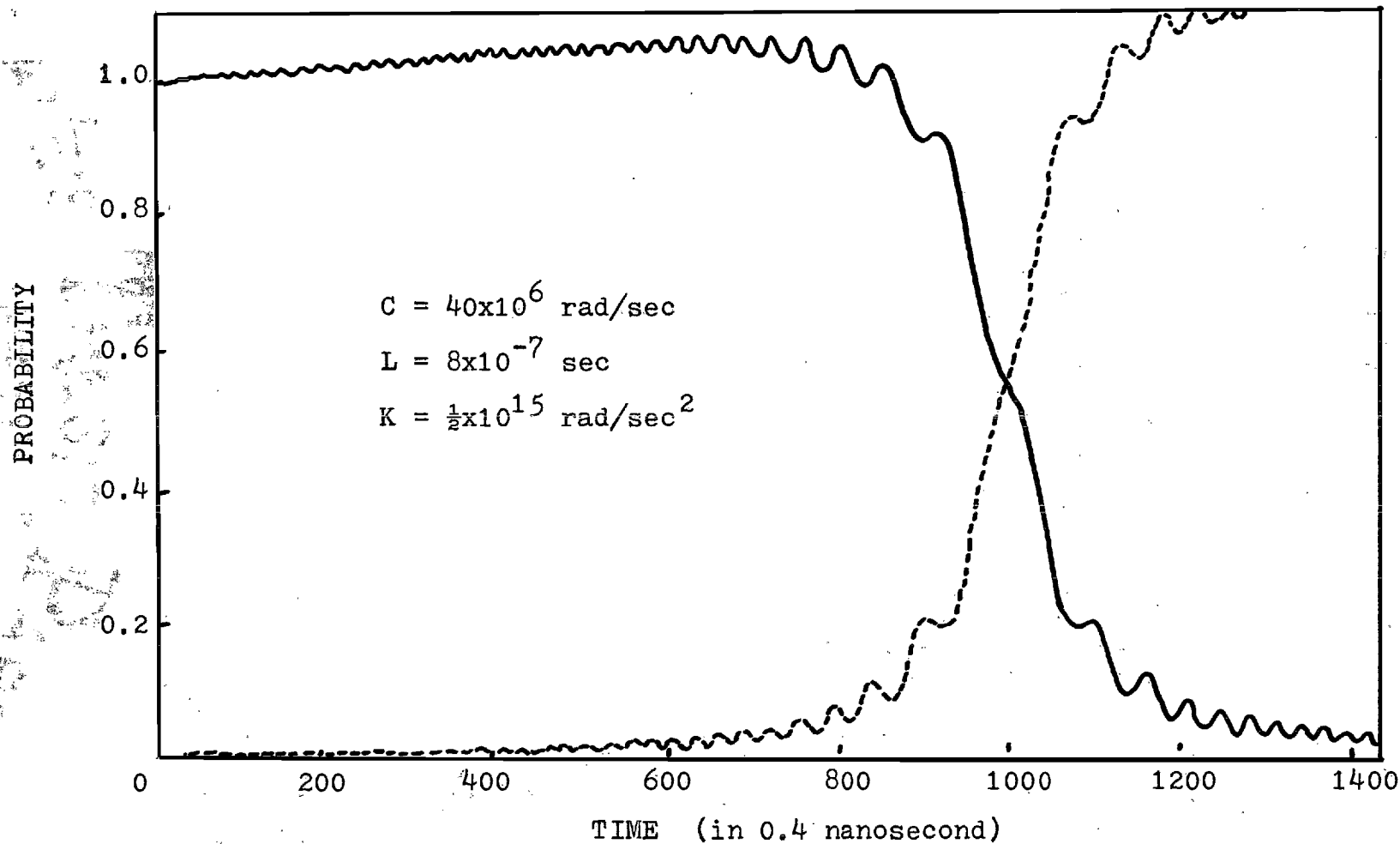


Figure 10. Ground and Excited State Populations during Adiabatic Rapid Passage, Slower Sweep Rate.

did not remain normalized because of cumulative errors in the calculation. Figure 8 shows the effect of reducing the power to one half that used in the ideal case of Figure 6. The initial oscillation is very small, however it becomes larger at the final stage of sweep. The reversal process is not complete. Figure 9 shows a much faster (four times the ideal case) sweep rate; the reversal is not complete and terminates at 0.75 and 0.275. Figure 10 shows a slower sweep rate, i.e., only half that of the ideal case. The reversal is complete and there is essentially no change in oscillations compared with the ideal case.

#### Stark Sweep Method

In this investigation the experimental method used for sweeping through the resonance frequency was somewhat different from that in the above discussion. The microwave radiation frequency was held constant and the resonance frequency was swept through the fixed radiation frequency by use of the Stark effect.

Figure 11 shows the idea of this sweep through mechanism. The dashed line represents the magnitude of the Stark field as a function of time, and the solid lines trace the frequencies of the three Stark components of the ammonia line as functions of time. The horizontal solid line labeled  $\nu_k$  shows the klystron frequency which is held fixed. Just before time  $t_0$  the Stark field is on, Stark component 3 is

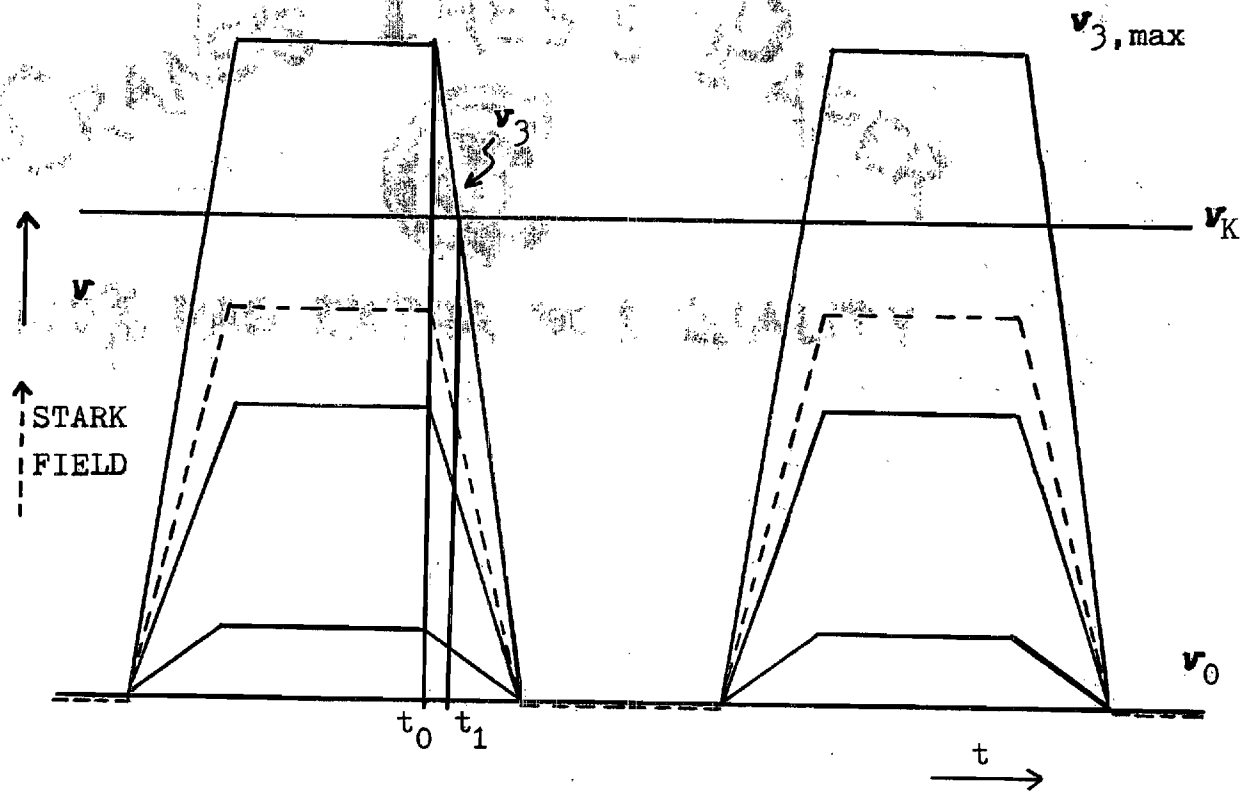


Figure 11. Relation between Stark Field, Frequency of Stark Components and Frequency of Klystron.

above  $\nu_k$ , and the ammonia gas has reached thermal equilibrium for these conditions. At  $t_0$  the Stark field begins to decrease, and at time  $t_1$  the third Stark component frequency  $\nu_3$  passes through the klystron frequency  $\nu_k$ . This interchanges the populations of the two levels associated with component 3, and the molecules begin to radiate at the frequency  $\nu_3$  which quickly falls to  $\nu_0$ , the zero field frequency of the rotational line. When this molecular radiation and the klystron radiation reach the crystal detector the output signal is the beat between the two at frequency  $\nu_k - \nu_0$ . This signal will decay quickly because of collisions with other molecules and with the walls of the absorption cell, and thermal equilibrium is quickly restored. As the Stark voltage rises there will be a similar excitation of the ground state molecules when  $\nu_3$  sweeps through  $\nu_k$  followed by molecular radiation whose frequency quickly rises to  $\nu_{3,max}$ . This radiation will beat with  $\nu_k$  giving an output signal from the crystal detector at frequency  $\nu_{3,max} - \nu_k$ .

## CHAPTER III

## EXPERIMENTAL PROCEDURE

General Experimental Apparatus

The equipment used in this investigation was a conventional Stark modulated spectrograph similar to the one described by Hughes and Wilson (4). Figure 12 shows a block diagram of this spectrograph.

Since the resonance frequencies of  $\text{NH}_3$  and OCS under investigation both fall in the range of 23 to 24 GHz, K-band microwave components were chosen. A universal klystron power supply was used for furnishing 2000 volts beam voltage and 12 ma beam current to a reflex klystron. This klystron then generated about 250 milliwatts microwave power to a load made up of the absorption cell, the detector and other units of the microwave line. A ferrite isolator was connected to isolate the klystron from the rest of the system. A necessary adjunct to any spectrometer is a means of measuring the frequency. This is usually determined approximately by means of a cavity wavemeter. Therefore a high-Q resonant cavity wavemeter was connected next to the ferrite isolator. A variable flap attenuator was also connected in the microwave line because it provided a simple convenient means of adjusting the power level and isolating source and load at the same time.

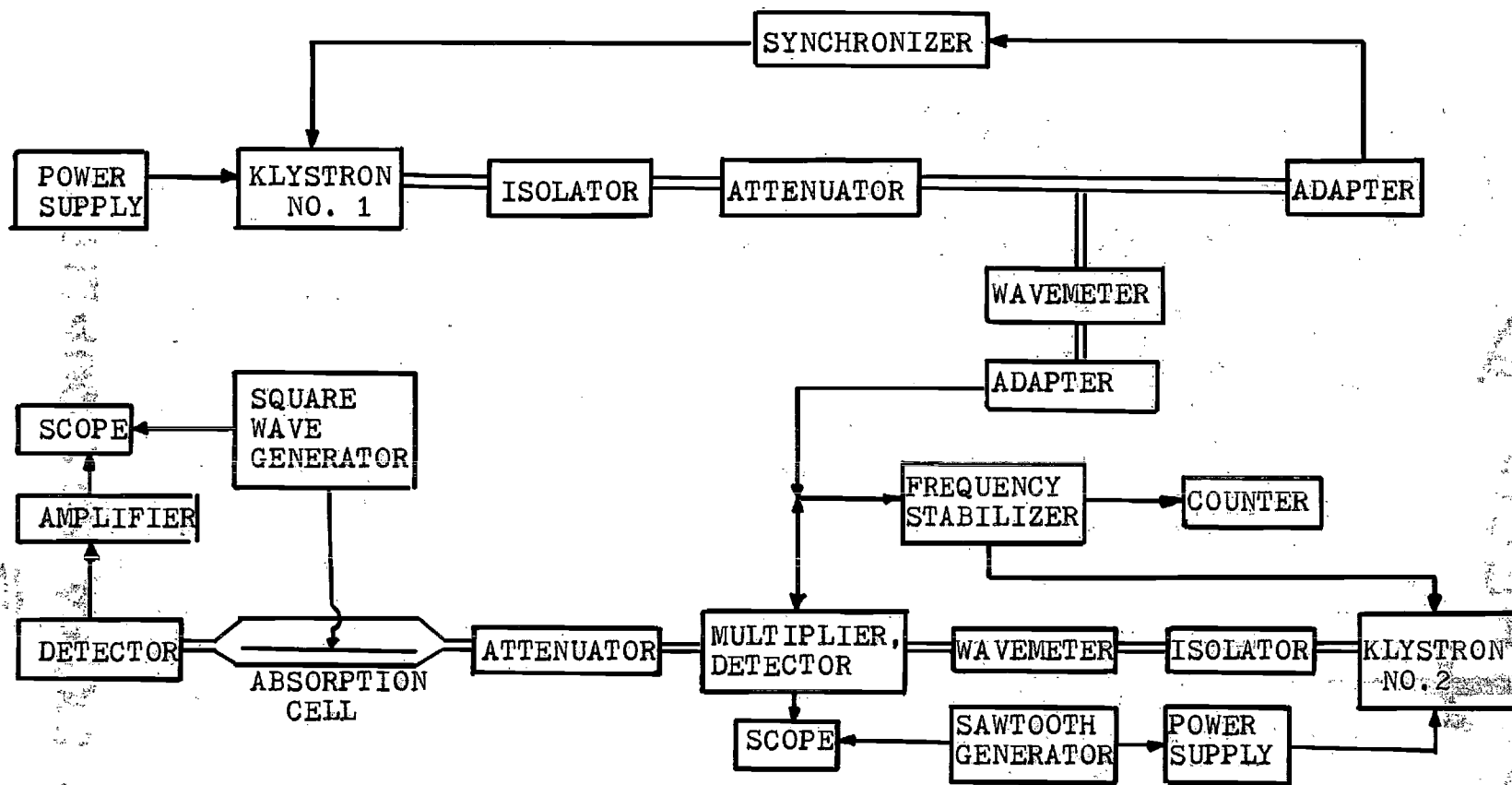


Figure 12. Block Diagram of Spectrograph.

The gas sample under investigation filled a 70 inch long brass K-band waveguide absorption cell. The absorption cell served a two-fold function: as a container for the sample gas and a medium for the transmission of microwave energy. In order to have the Stark components sweep through the microwave frequency, an 85-kHz squarewave voltage was applied to a flat strip electrode centered within the waveguide which produced an electric field parallel to the microwave electric field. This squarewave voltage was produced by an 85-kHz, 0 to 2000 volts square wave generator.

The signal from the absorption cell was detected by a crystal diode mounted at the end of the cell. A broadband amplifier using an integrated circuit was then added to the microwave line to amplify the beat signal from the crystal detector. A dual trace oscilloscope was used to display the signal output, the ideal exponential curve which will be discussed in the next section and the rise and fall of the Stark voltage.

Since the microwave radiation from the klystron was required to have a fixed frequency, a lock-in system was added to the microwave line for this purpose. This system, similar to that described by Nave (5), uses both phase-lock stabilization plus discriminator stabilization.

An oscillator-synchronizer was used to provide the first stage phase-lock stabilization. Its function can be described as follows. The klystron signal is mixed with a

harmonic of the signal from a crystal RF reference oscillator to produce a 30 MHz IF signal. This IF signal is then phase compared to an IF reference signal from an internal crystal controlled oscillator. Once it is locked, any attempt by the klystron to shift frequency will immediately produce a phase error and a phase comparator output voltage. That voltage is then applied in series with the klystron's reflector voltage to stop the frequency shift. In the arrangement shown in Figure 12, klystron number one is stabilized at a fixed frequency as described above.

The frequency of the stabilized klystron is then doubled (or tripled) and this signal is mixed with the output of klystron number two in a crystal multiplier-mixer to produce a 60 MHz beat note. The output of the crystal multiplier is applied to a microwave frequency stabilizer which consists of an IF amplifier, a discriminator and a DC amplifier. The output of the DC amplifier is applied in series with the klystron reflector voltage to stabilize the klystron. The discriminator will lock on to harmonics at 50 MHz intervals up to 12 GHz. That is, a variation in the klystron frequency will produce an error voltage at the discriminator which keeps the klystron frequency about 60 MHz from one of the harmonic frequencies.

As an example of the lock-in procedure, consider the case of the (3,3) inversion line of  $\text{NH}_3$  at 23870.12 MHz. The lock-in arrangement is shown on Figure 13. The first

klystron is stabilized by the oscillator synchronizer at 11910 MHz by locking it 30 MHz above the 108th multiple of the 110 MHz RF reference oscillator in the stabilizer. This 11910 MHz signal is then doubled by the crystal multiplier-mixer and becomes 23820 MHz. Since the second klystron is tuned to 23878.12 MHz, there is a 58.12 MHz beat note which is applied to the microwave frequency stabilizer. The discriminator is adjusted so that a beat note of 58.12 MHz will lock the second klystron at exactly 23878.12 MHz, which is 8 MHz above the  $\text{NH}_3$  inversion line.

#### Data Collection Procedure

The pressure measurement has been a very important factor in this investigation. Three types of pressure gauges were used. A Pirani gauge, which must be calibrated for each individual gas, was used only as a reference for indicating the rough reading. An MKS Baratron Electronic Pressure Meter which measures pressures in the vacuum range independent of the gas composition, was the main pressure measurement apparatus used. A precise MacLeod gauge was used to calibrate the MKS Baratron gauge.

Most of the data were taken with the absorption cell at  $-80^\circ\text{C}$ , which was obtained by placing dry ice directly on the absorption cell. There are two reasons for doing this. First, both rotational lines,  $\text{NH}_3(3,3)$  and  $\text{OCS}(J = 1 \text{ to } 2)$ , are low- $J$  transitions therefore their intensities are greater

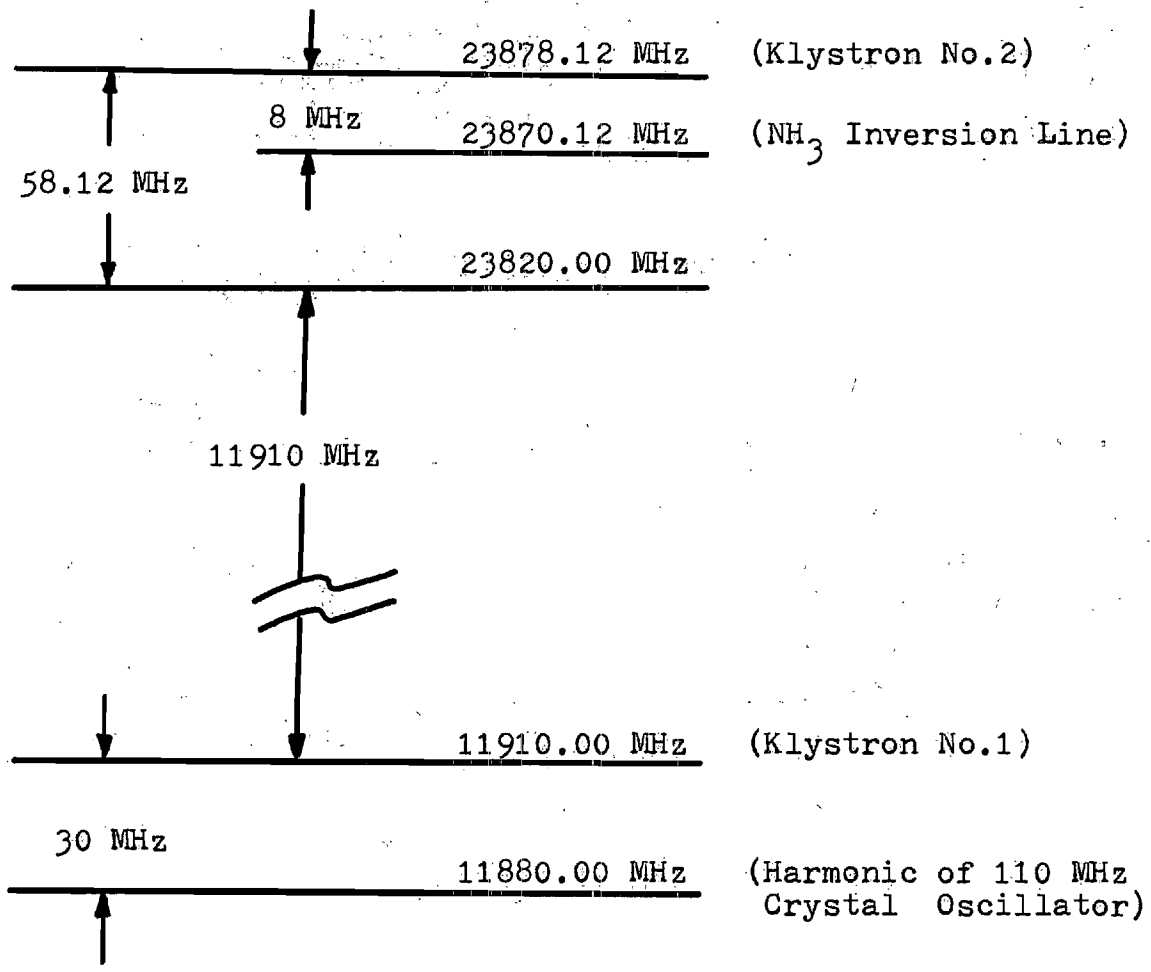


Figure 13. Relation of the Frequencies Used in the Frequency Lock-in System.

THE  
 NATIONAL BUREAU OF STANDARDS  
 U.S. DEPARTMENT OF COMMERCE  
 WASHINGTON, D.C. 20540

at low temperature. Second, the  $\text{NH}_3$  pressure seems to be more stable at this low temperature. The sample gas, at room temperature was introduced into the cooled absorption cell. The gas source was then shut off and the sample in the absorption cell allowed to condense down to its vapor pressure. The absorption cell was then pumped until the desired pressure was reached. Data were taken after waiting long hours for the cell to cool down, for the gas to saturate the cell and for the gas pressure to stabilize at the desired low pressure when pumped out.

For the fast passage type of excitation precise adjustment of the power level is not necessary in order to observe a signal. The microwave power was attenuated by a calibrated variable attenuator in front of the absorption cell until an optimum beat signal pattern was seen on the oscilloscope. This optimum power was measured by a power meter. The emission radiation power was measured by comparing its signal amplitude with that of a source of known power. This technique will be discussed in detail in the next chapter.

One of the measurements made in this study was the decay rate of the emission radiation. In order to measure the exponential decay rate precisely the RC-circuit shown in Figure 14 was used to display an exponential decay curve on the oscilloscope. The input to the circuit is the square wave from the oscilloscope gate and the output of the circuit is connected to one of the vertical displays. This ideal

exponential decay was superimposed on each peak of the beat signal. By changing the 2.5 K variable resistor, which has a dial reading for precise measurement, a different rate of decay can be obtained for matching to each peak of the beat signal. The actual time constant in nano-seconds was found by using the calibration chart shown in Figure 15. Note on

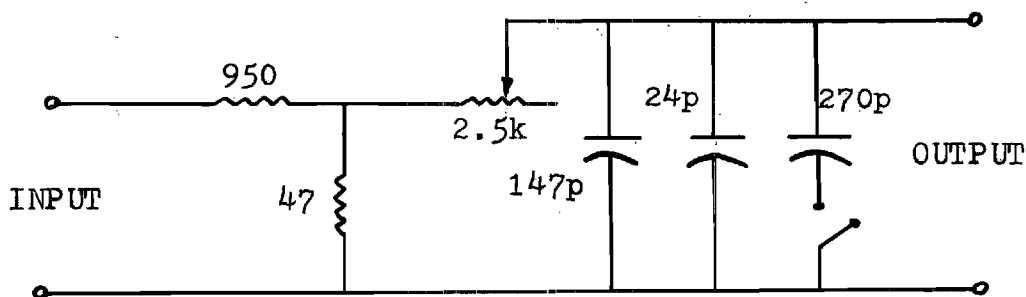


Figure 14. RC-circuit Used for Measuring the Time Constant.

the chart two methods have been used for calibrating the RC-circuit time constant. In one case a Wheatstone bridge and a capacitance bridge were used to measure the variable resistor and the capacitors respectively. The product of these R and C values is plotted with a solid line in Figure 15 designated by RC. In the other case a Polaroid camera was used to photograph the exponential decay curve on the oscilloscope and the time constant was measured directly on the

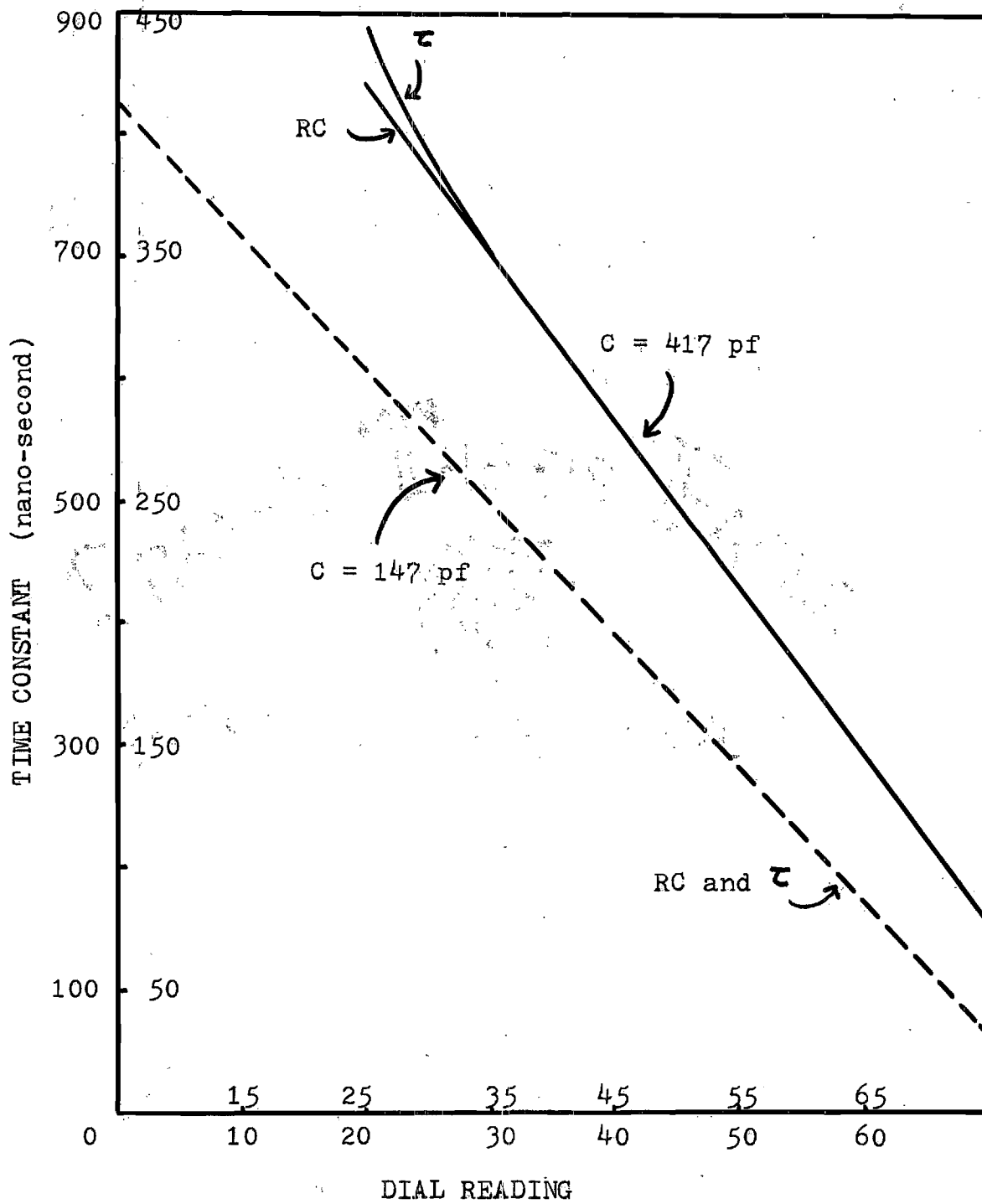


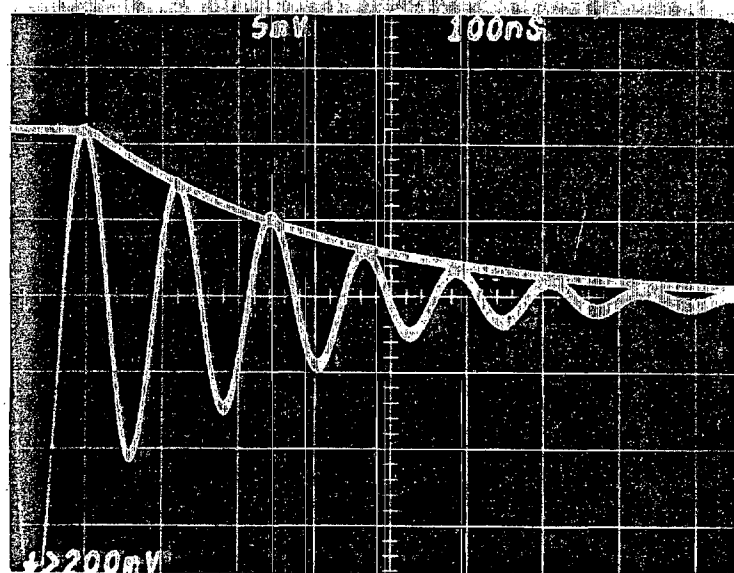
Figure 15. Relation between Time Constant and Dial Reading

photograph. The results of these measurements are shown by the curve designated by  $\tau$  in the same figure. The dashed line applies when only one capacitor ( $C = 147\text{pf}$ ) is used, and goes with the lower range of time constants. As can be seen from the figure both methods give the same results except for time constants greater than 700 nano-seconds.

In some cases, especially when more than one Stark component passes through the klystron frequency the envelope of the beat signal does not show an ideal exponential decay and it becomes difficult to match with the exponential RC-decay. It was found that, instead of matching the exponential decay from the first positive peak, matching from the second positive peak will give much better results as shown on Figure 16.



(a) With First Positive Peak



(b) With Second Positive Peak

Figure 16. Matching of the Exponential Curve with Different Peaks.

## CHAPTER IV

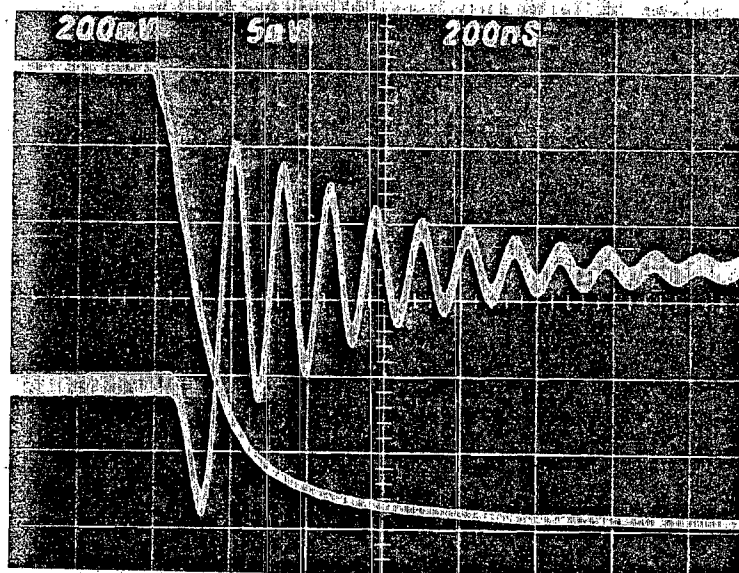
## RESULTS OF THE INVESTIGATION

Observation of Microwave Emission under Different Conditions

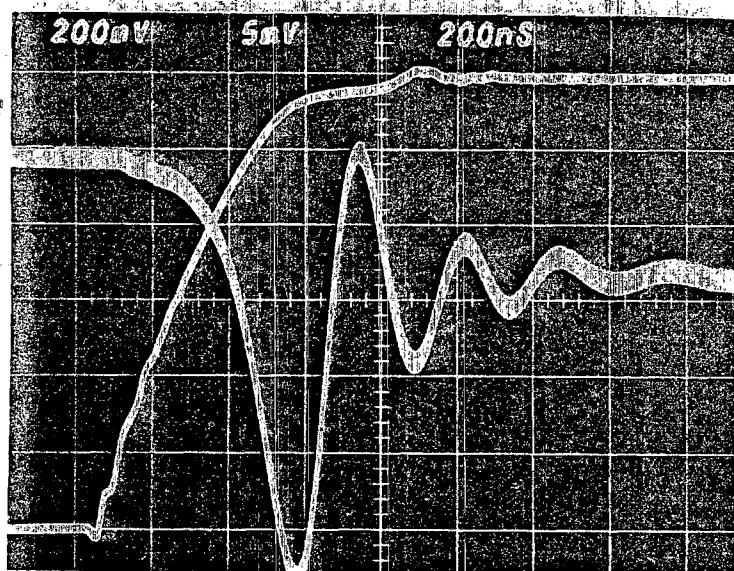
The nature of the microwave radiation following the sweep of a Stark component through the klystron frequency can be best described by showing simultaneous oscilloscope tracings of the Stark voltage and the crystal detector signal. Therefore, a series of photographs of the dual trace oscilloscope is presented on the following pages which shows qualitatively the effects of varying the conditions of observation. The quantitative results will be discussed in the next section of this chapter.

Eighteen photographs (Figures 17 to 24) were made at ammonia and OCS gas pressures between 2 and 150 microns. The rise and fall times for the Stark voltage are about 0.5 microseconds, and the klystron power used was about 5 milliwatts. The klystron frequency was usually fixed about 5 to 8 MHz away from the rotational lines. Unless otherwise specified the molecules under investigation were cooled to dry ice temperature, i.e.,  $-80^{\circ}\text{C}$ .

Figure 17(a) shows the signal after the Stark component sweeps down through the klystron frequency, and Figure 17(b) shows the signal after the Stark component sweeps up



(a) Fall



(b) Raise

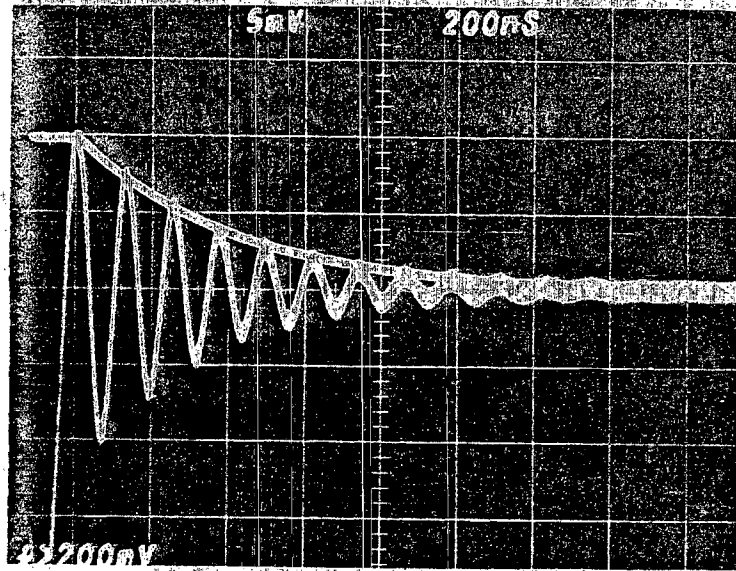
Figure 17. Observation of Microwave Emission under Raising and Falling Stark Voltage.

through the klystron frequency. The oscillatory signal is the beat between the frequencies of the molecular radiation and the klystron radiation. The larger beat frequency observed in 17(a) is due to the fact that the klystron frequency is fixed farther from the rotational line frequency than it is from the Stark component frequency.

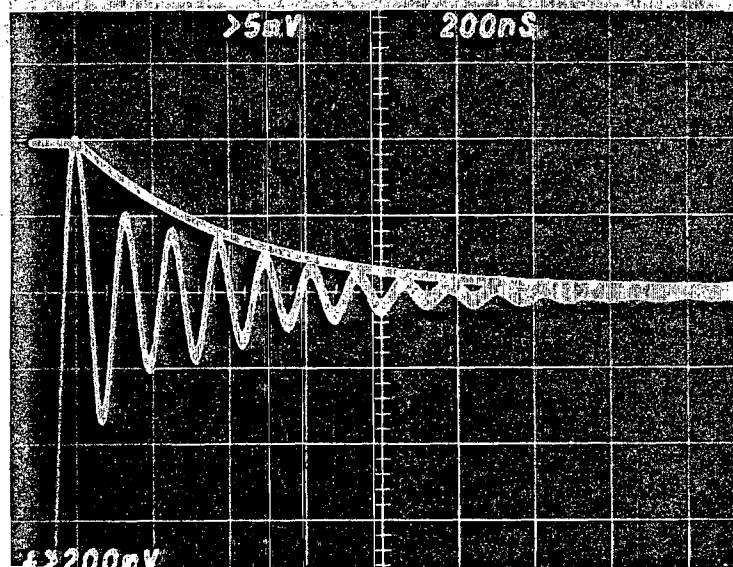
Figure 18(b) shows the effect of sweeping two Stark components through the klystron frequency almost simultaneously. In order to determine the decay rate of the molecular radiation the Stark voltage trace has been replaced by an RC exponential decay curve. The photograph 18(a) shows that, for a low Stark voltage and one Stark component, the decay is a nearly perfect exponential, but for a higher Stark voltage and two Stark components the decay is not exponential. This is presumably the result of an overlap of signals due to the two components. The photographs were taken at 30 microns pressure and 1087 volts/cm Stark field.

Figure 19 shows the effect of reducing the sweep rate. The sweep is about ten times slower in 19(a) and the radiated pulses from the separate Stark components are almost completely separated. The slow sweep was produced by a transistorized square-wave generator constructed for this purpose. Ammonia gas was used under 12.4 microns pressure and 2174 volts/cm Stark field for photograph 19(b).

Figure 20 shows the beat signal under two opposite extremes of klystron power. A very small amount of micro-

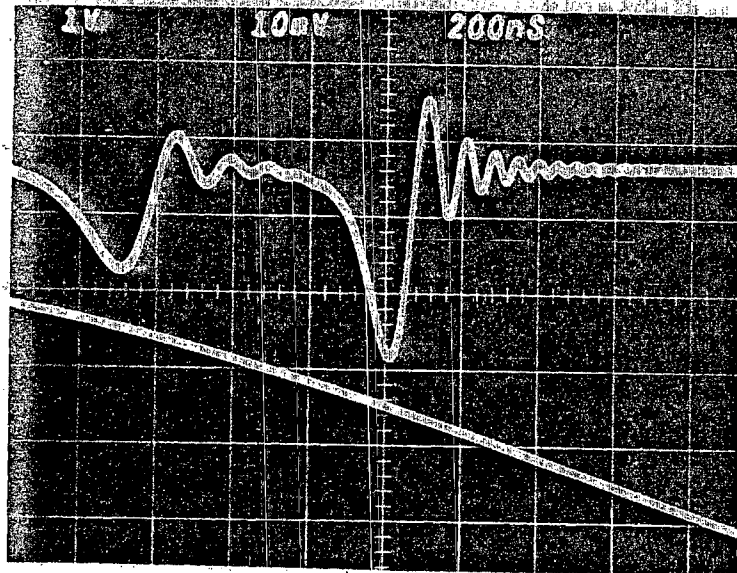


(a) One Component

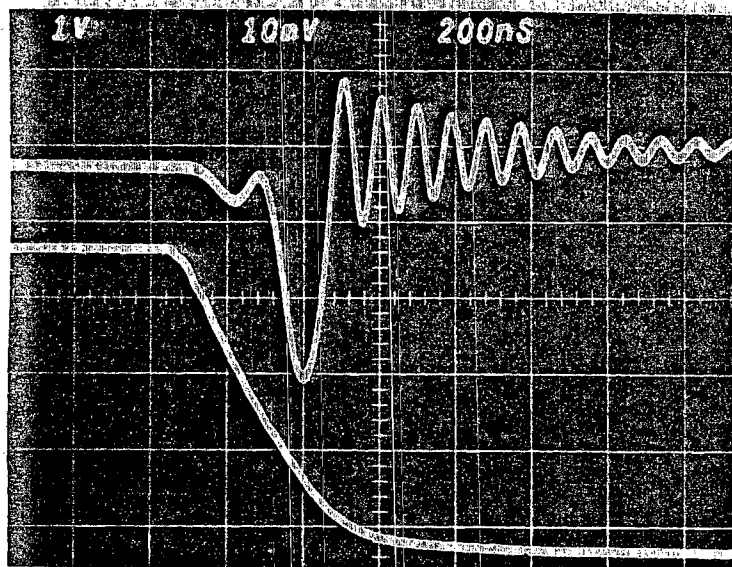


(b) Two Components

Figure 18. Observation of Microwave Emission under Different Number of Stark Components.

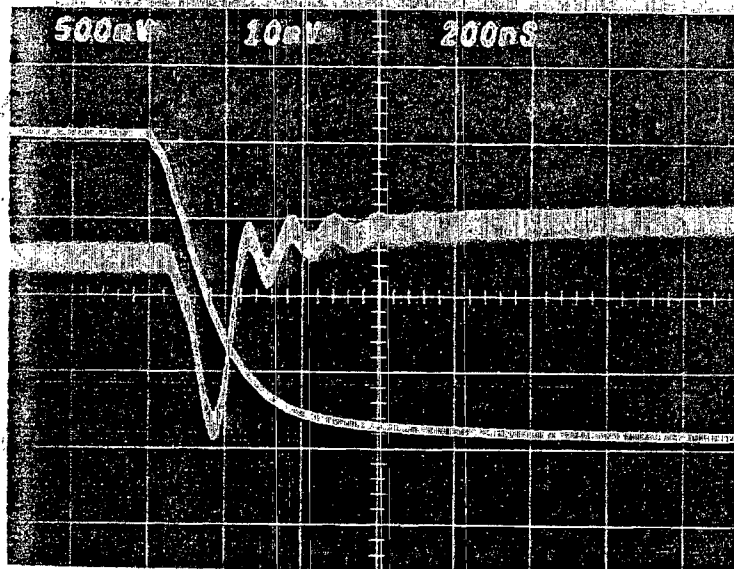


(a) Slow Sweep

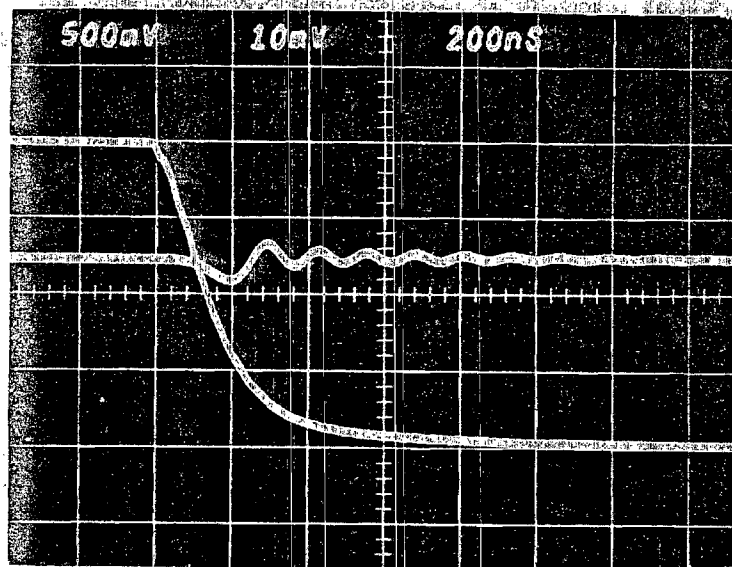


(b) Fast Sweep

Figure 19. Observation of Microwave Emission under Different Sweep Rate.



(b) - Over Saturated Power

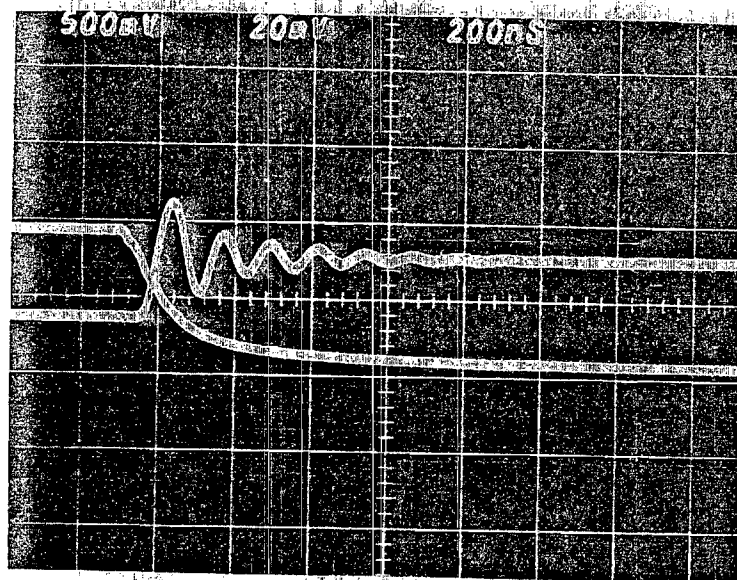


(a) Very Small Amount of Power

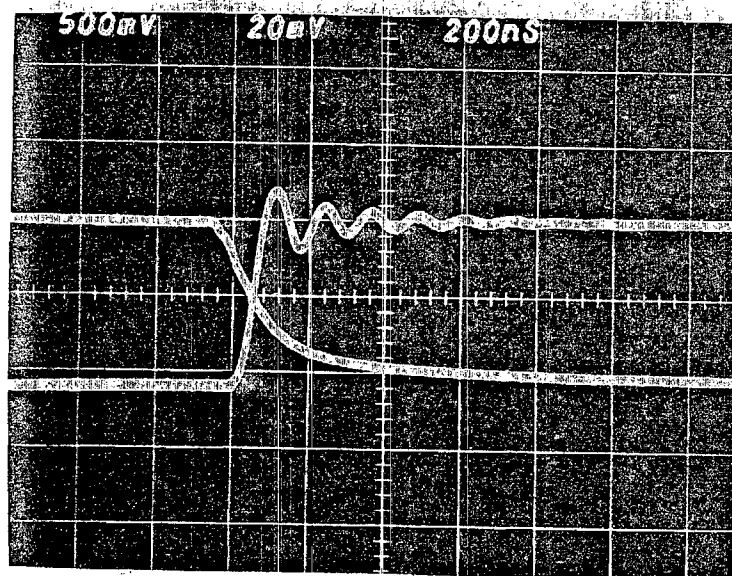
Figure 20. Observation of Microwave Emission under Two Opposite Extremes of Klystron Power.

wave power was transmitted through the ammonia gas in 20(a) and a power much larger than the optimum was used in 20(b). An approximately 250 milliwatt microwave power was generated by the klystron which was attenuated about 1 db through a variable attenuator before it was transmitted into the absorption cell. The optimum power was obtained when the variable attenuator was turned to 12 db and the resulting signal is shown in Figure 17(a). The photographs of Figure 20 were taken at 30 micron pressure and 1087 volts/cm Stark field.

Figure 21 has six photographs to show the emission under six different Stark fields. Photograph (a) shows the signal produced when a Stark voltage of 80 volts was applied to the electrodes (with a separation of 0.184 cm). This was barely enough Stark voltage to produce a small signal. Only the upper edge of the broadened Stark component (number three in Figure 11) was being swept up to the klystron frequency. When the voltage was increased to 100 volts, photograph (b), the center of the broadened Stark component was swept up to the klystron frequency and the offset of voltage on and voltage off base lines is maximum because of the absorption which occurred when the voltage was on. At 140 volts, photograph (c), the maximum absorption and maximum dip of the signal occurs after the Stark voltage starts to drop and the excitation mechanism is now adiabatic rapid passage. The offset of base lines here is the result of absorption by the

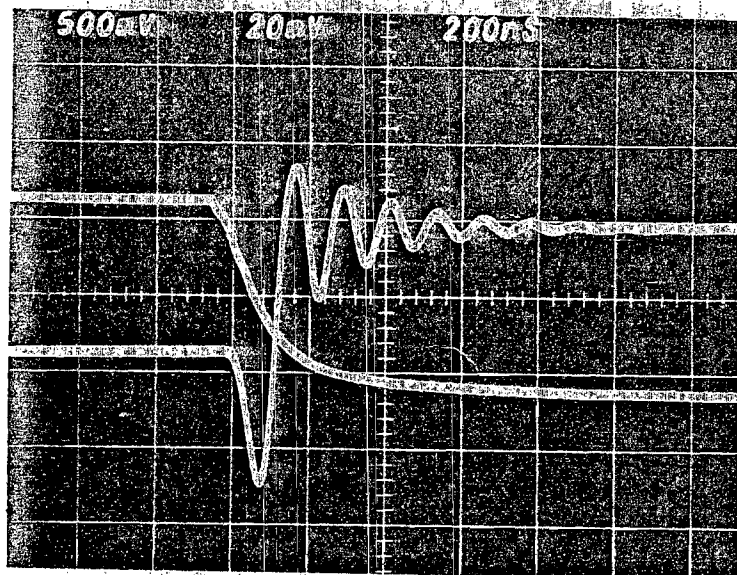


(a) 80 Volts

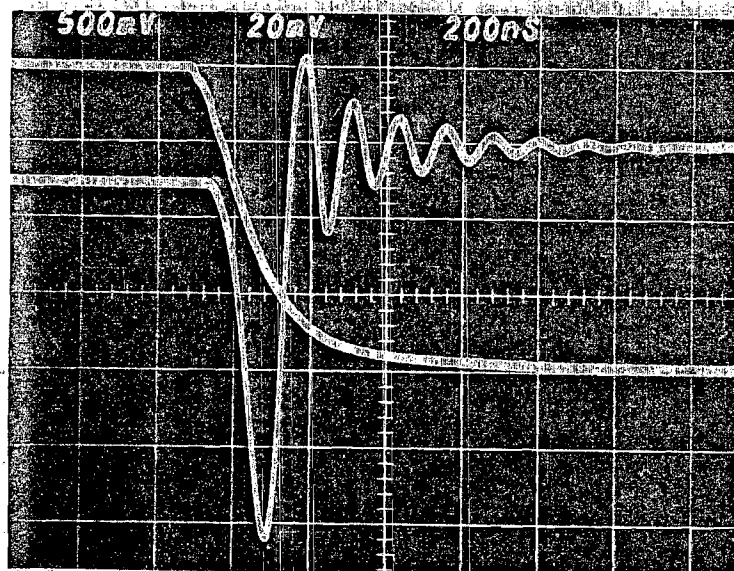


(b) 100 Volts

Figure 21. Observation of Microwave Emission under Different Stark Voltages.



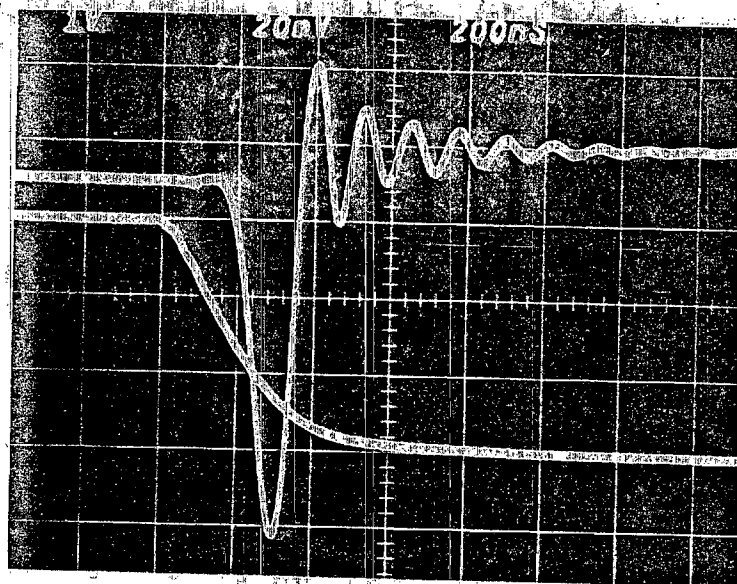
(c) 140 Volts



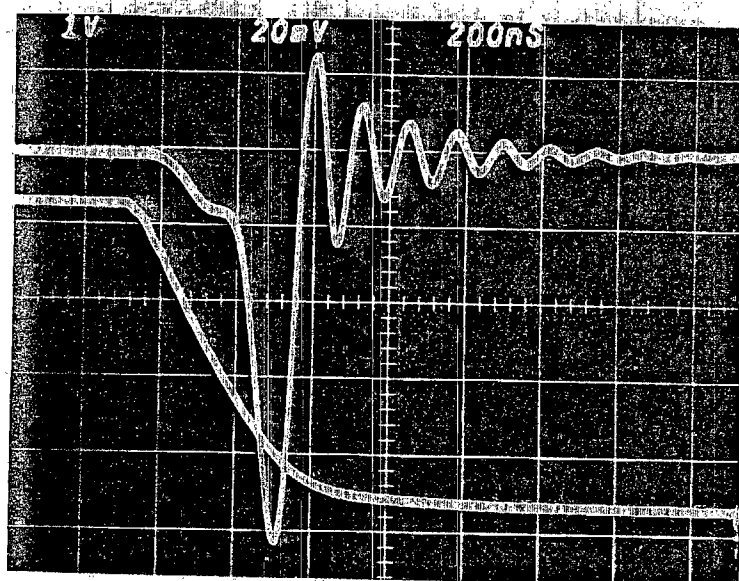
(d) 200 Volts

( continued )

Figure 21. Observation of Microwave Emission under Different Stark Voltages.



(e) 300 Volts



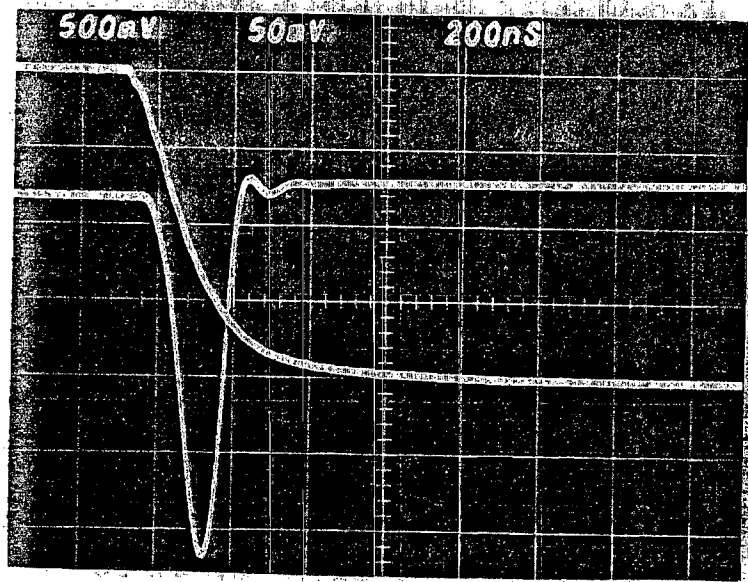
(f) 400 Volts

( continued )

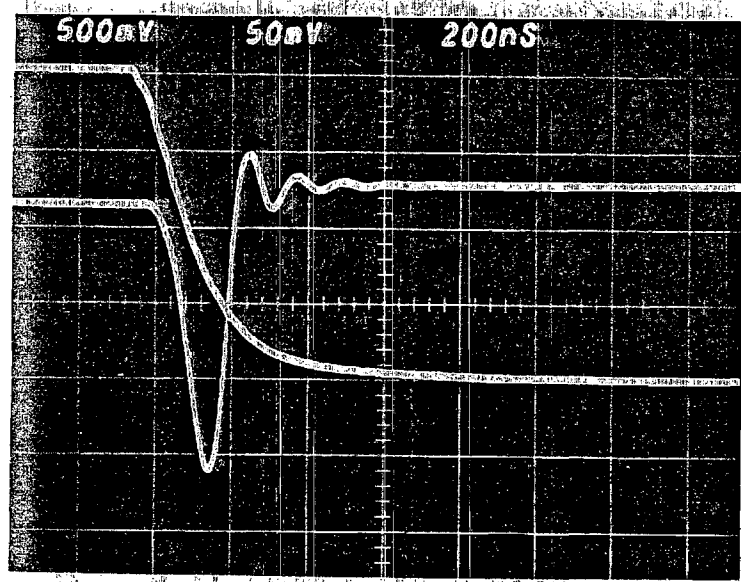
Figure 21. Observation of Microwave Emission under Different Stark Voltages.

lower edge of component three and the upper edge of component two before the voltage started to drop. When the Stark voltage was increased to 200 volts the signal amplitude reached its maximum and very clear oscillation is shown on photograph (d). The base line offset is now very small since none of the Stark components fall near the klystron frequency when the voltage is on. At 300 volts, from photograph (e) one sees that the third Stark component is about to enter and can be seen on the left of the beat signal. On photograph (f) the third Stark component is more clearly visible and makes the ripple on the left portion of the beat signal as the Stark voltage increased to 400 volts. For comparison the Stark fields for Stark voltages 80v, 100v, 140v, 200v, 300v, and 400v used in Figure 21 are 435 v/cm, 543 v/cm, 761 v/cm, 1087 v/cm, 1630 v/cm, and 2174 v/cm respectively. The sample was ammonia at a pressure of 30 microns and the klystron was fixed about 8 MHz above the  $\text{NH}_3$  (3,3) line.

Figure 22 shows the effect of changing the ammonia gas pressure with other conditions constant. For pressures above about 150 microns the signal decays because of collisions before many oscillations can occur. This can be seen on photograph (a) where just one ripple appears. When the pressure was reduced to 70 microns as shown on photograph (b), the oscillations began but it was difficult to measure the decay rate from so few ripples. At 20 microns as shown on photograph (c), the exponential decay is well formed after

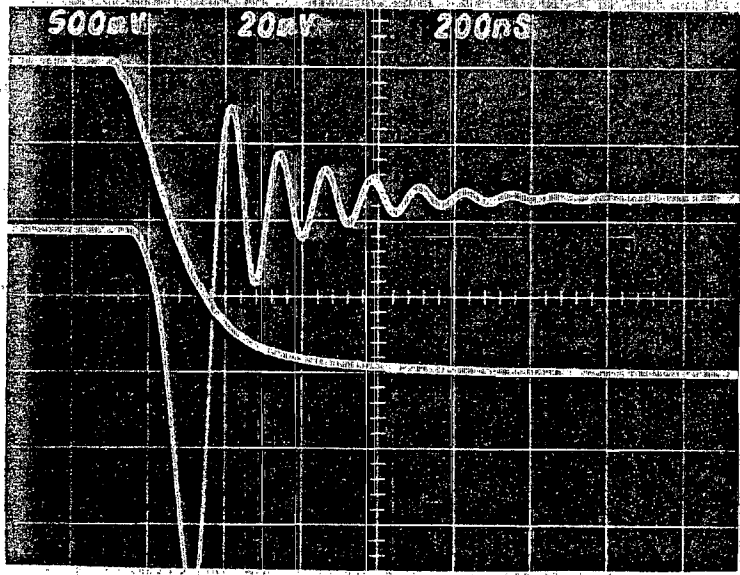


(a) 150 Microns

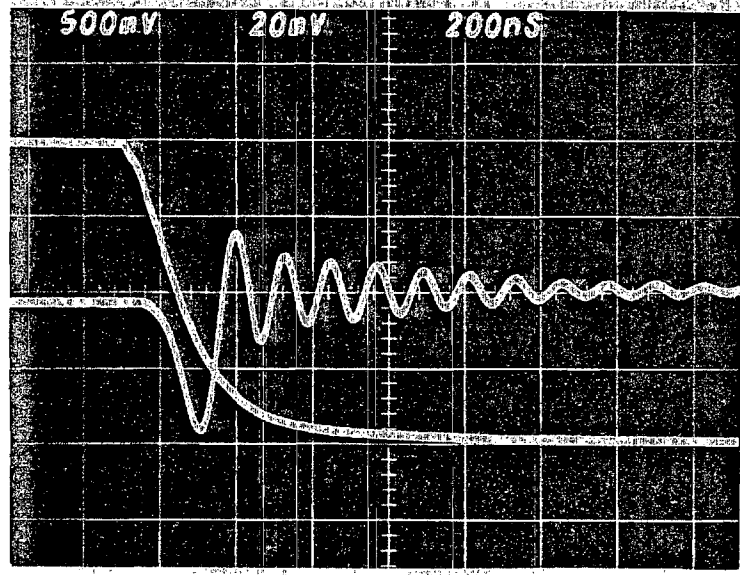


(b) 70 Microns

Figure 22. Observation of Microwave Emission under Different Pressures.



(c) 20 Microns



(d) 2 Microns

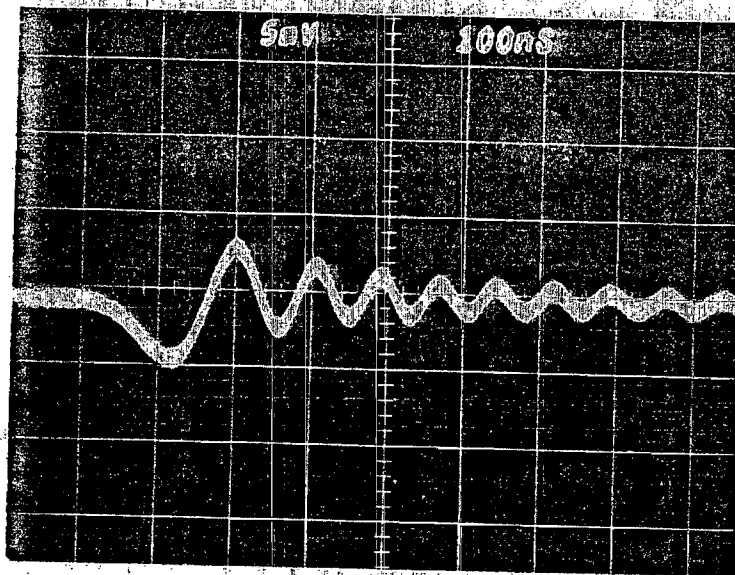
( continued )

Figure 22. Observation of Microwave Emission under Different Pressures.

the first dip. As the pressure goes down to only 2 microns the exponential decay is very slow because collisions are infrequent. The time constant is inversely proportional to pressure as will be explained in detail in the next section. The signal amplitude is slightly reduced in going from 20 to 2 microns pressure as shown on photograph (d). The Stark field used for the photographs in Figure 22 was 1087 volts/cm and the klystron was fixed at 8.01 MHz above the  $\text{NH}_3$  (3,3) line.

Figure 23 shows the signal produced by OCS at two different temperatures. Photograph (a) shows the signal from OCS at room temperature while photograph (b) shows the signal at dry ice temperature, i.e.,  $-80^\circ\text{C}$ . As can be seen from Figure 23, the beat signal is smaller when the sample is at the higher temperature. This is because the low-J transitions are more heavily populated at the lower temperature, and the transition involved here is the OCS  $J = 2 \rightarrow 1$ . The Stark field applied was 3265 volts/cm and the klystron frequency was fixed 5 MHz above the OCS  $J = 2 \rightarrow 1$  rotational line.

Figure 24 shows the signals from  $\text{NH}_3$  and OCS at the same low pressure 10 microns. The  $\text{NH}_3$  signal is stronger because its larger dipole moment produced a stronger molecular radiation. The  $\text{NH}_3$  signal decays more quickly for the same reasons. That is, the larger dipole moment causes a stronger interaction between molecules which is responsible



(a) Room Temperature



(b) Dry Ice Temperature

Figure 23. Observation of Microwave Emission under Different Temperature.

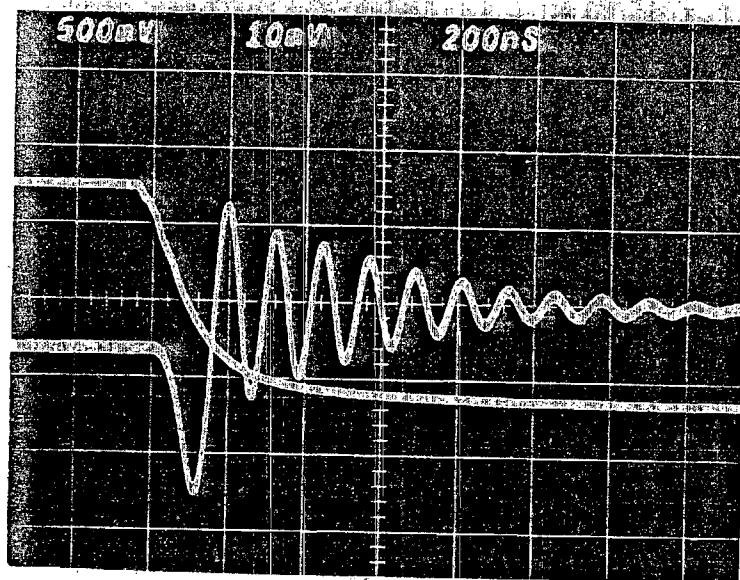
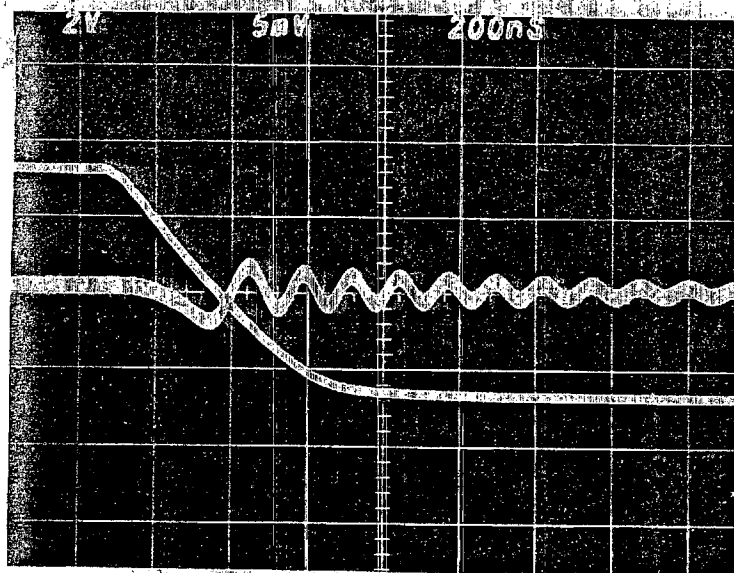
(a)  $\text{NH}_3$ (b)  $\text{OCS}$ 

Figure 24. Observation of Microwave Emission under Different Samples at Low Pressures.

for the decay.

When one attempts to match an exponential decay curve to the  $\text{NH}_3$  signal it is not unusual to find a small deviation of the  $\text{NH}_3$  signal from an exponential decay. The amplitude of the  $\text{NH}_3$  signal will fall then rise slightly then fall again producing a small bump in the envelope. The bump is more prominent at low pressures and may be connected with the fact that the decay rate for the  $\text{NH}_3$  signal is slower than expected. Such a bump is not observed for OCS.

#### The Relation of Decay Rate and Other Physical Parameters

From observation of the microwave emission it was found that the crystal detector output signal, i.e., the beat between the molecular and klystron radiations decays quickly and approximately exponentially due to collisions with other molecules and with the walls of the cell. By changing the environmental physical parameters, such as pressure, temperature and power it was found that there are certain relationships between these parameters and the decay rate. The measurement and analysis of these relationships are discussed below.

##### Pressure

The decay rate of the microwave emission is closely related to the broadening of rotational lines with increasing pressure. From kinetic theory of gases it is known (6) that the mean time  $\tau$  between collisions of molecules may be related

to the molecular diameter  $b$  by the equation

$$\tau = \frac{1}{N \bar{v}_{12} b^2} \quad (12)$$

Where  $N$  is the number of molecules per unit volume and  $\bar{v}_{12}$  is the mean relative velocity of the colliding molecules. For a fixed temperature,  $\bar{v}_{12}$  and  $b$  are constant while  $N$  is proportional to the pressure. Since  $\tau = 1/(2\pi\Delta\nu)$  (7) where  $\Delta\nu$  is the half line width at half-maximum power, and assuming that  $N = CP$  where  $C$  is a constant at a particular temperature and  $P$  is the pressure it is found that

$$\frac{\Delta\nu}{P} = \frac{C \bar{v}_{12} b^2}{2} = \Delta\nu_p \quad (13)$$

Townes, Holden and Merritt (8) were the first group to measure this line-breadth parameter  $\Delta\nu_p$ . For the OCS  $J = 2 \rightarrow 1$  transition at room temperature they report the value  $\Delta\nu_p = 6.0 \pm 1$  Mc/mm-Hg. Several years later Feeny Lackner, Moser and Smith (9) applied the same experimental method, i.e., directly measured the difference in frequency between the two sides of the absorptional line at different pressures. They reported a value of  $6.40 \pm 0.10$  Mc/mm-Hg.

In this investigation the decay time  $\tau$  was measured for OCS and  $\text{NH}_3$  gases. The measurements on OCS were made in the pressure range from 20 to 200 microns of Hg, and the sample was stored in the absorption cell and cooled to dry ice

temperature. The klystron was locked at 24330.5 MHz which was 4.6 MHz above the  $J = 2 \rightarrow 1$  rotational line of OCS. The Stark field was 3265 Volts/cm furnished by a 600 volt square wave voltage. The data were taken at different pressures and the results are shown in Table 1 and plotted in Figure 25. The second column of Table 1 indicates the relative signal strength of the first oscillation measured in millivolts from center to first positive peak. The values of  $1/\tau$  given in the last column of Table 1 are plotted versus the pressure in Figure 25. The slope of this line obtained by the method of least squares was found to be  $0.574 \times 10^{-4}$  nano-sec<sup>-1</sup> - micron<sup>-1</sup>-Hg.

In order to check the results for the decay rate of the signal with those of the line broadening measurements mentioned above a temperature correction, which will be discussed in the next section, was applied to the slope of the line of Figure 25. It was found that  $\frac{1}{\tau_p} = 0.373 \times 10^{-4}$  n-sec<sup>-1</sup> -micron-Hg at 25°C. From  $2\pi P\tau = 1$  it is then found

$$\frac{\Delta\nu}{P} = \frac{1}{2\pi\tau_p} = 5.9 \text{ Mc/mm-Hg} \quad (14)$$

which is very close to the value 6.0 Mc/mm-Hg reported by Townes and slightly smaller than the value 6.4 reported by Feeny (9).

Some difficulty was encountered in trying to repeat measurements of the type reported in Table 1. Figure 26

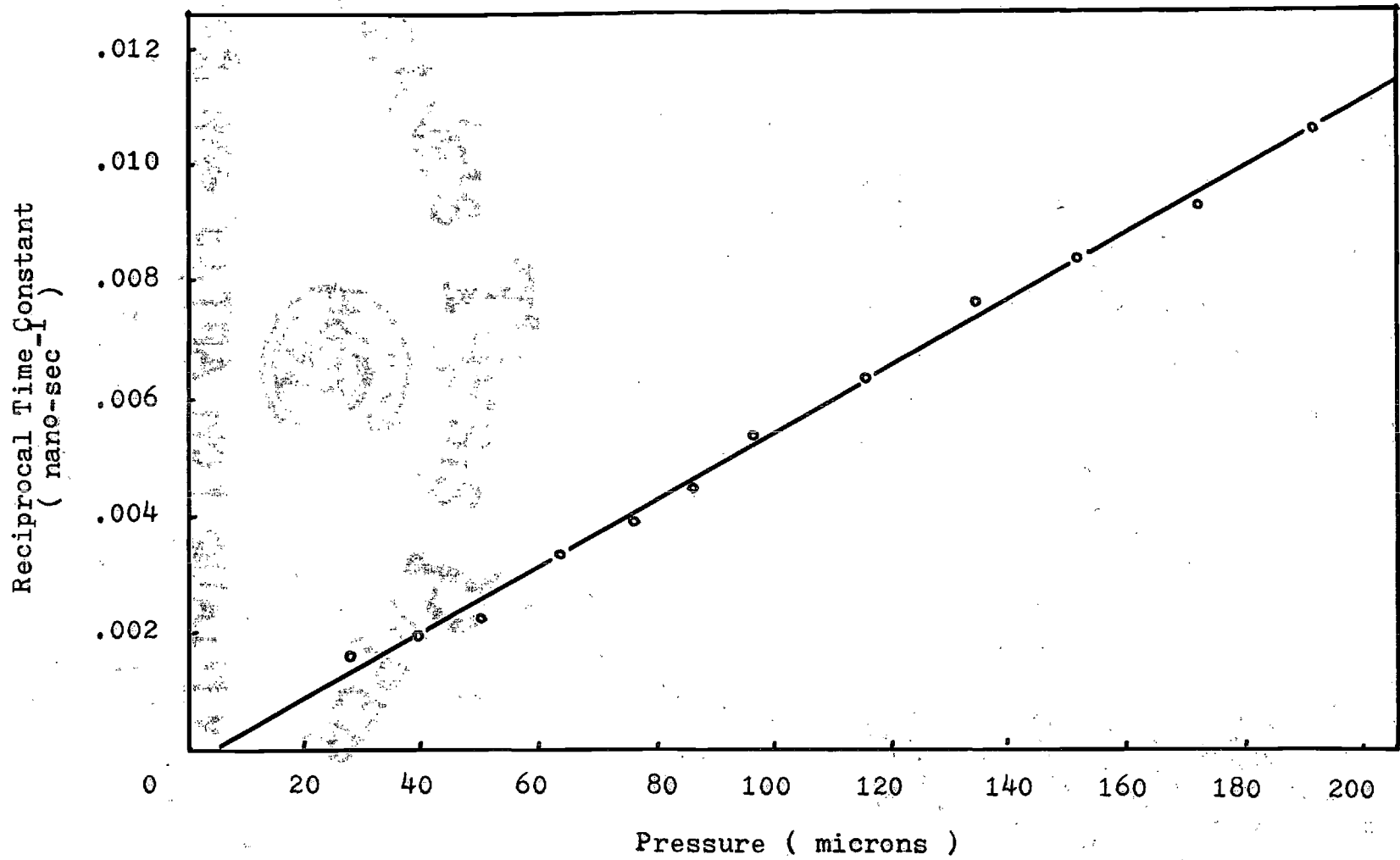


Figure 25. Reciprocal Time Constants versus Pressure, OCS J = 2 1, V = 0.

Table 1. Pressure, Signal Amplitude, and  
Time Constant of OCS  $J = 2 \rightarrow 1$

Pressure (Micron)	Signal Amplitude (Millivolt)	Time Constant (Nano-sec)	Reciprocal Time Constant (Nano-sec <sup>-1</sup> )
191.7	16.0	93	0.01075
172.5	16.5	107	0.00935
152.1	18.0	119	0.00840
135.1	18.5	130	0.00769
116.2	19.0	157	0.00637
96.9	18.5	187	0.00535
86.8	18.3	223	0.00448
76.8	17.5	257	0.00389
64.6	16.5	297	0.00337
51.0	14.5	445	0.00225
39.7	12.0	512	0.00195
28.2	9.5	624	0.00160

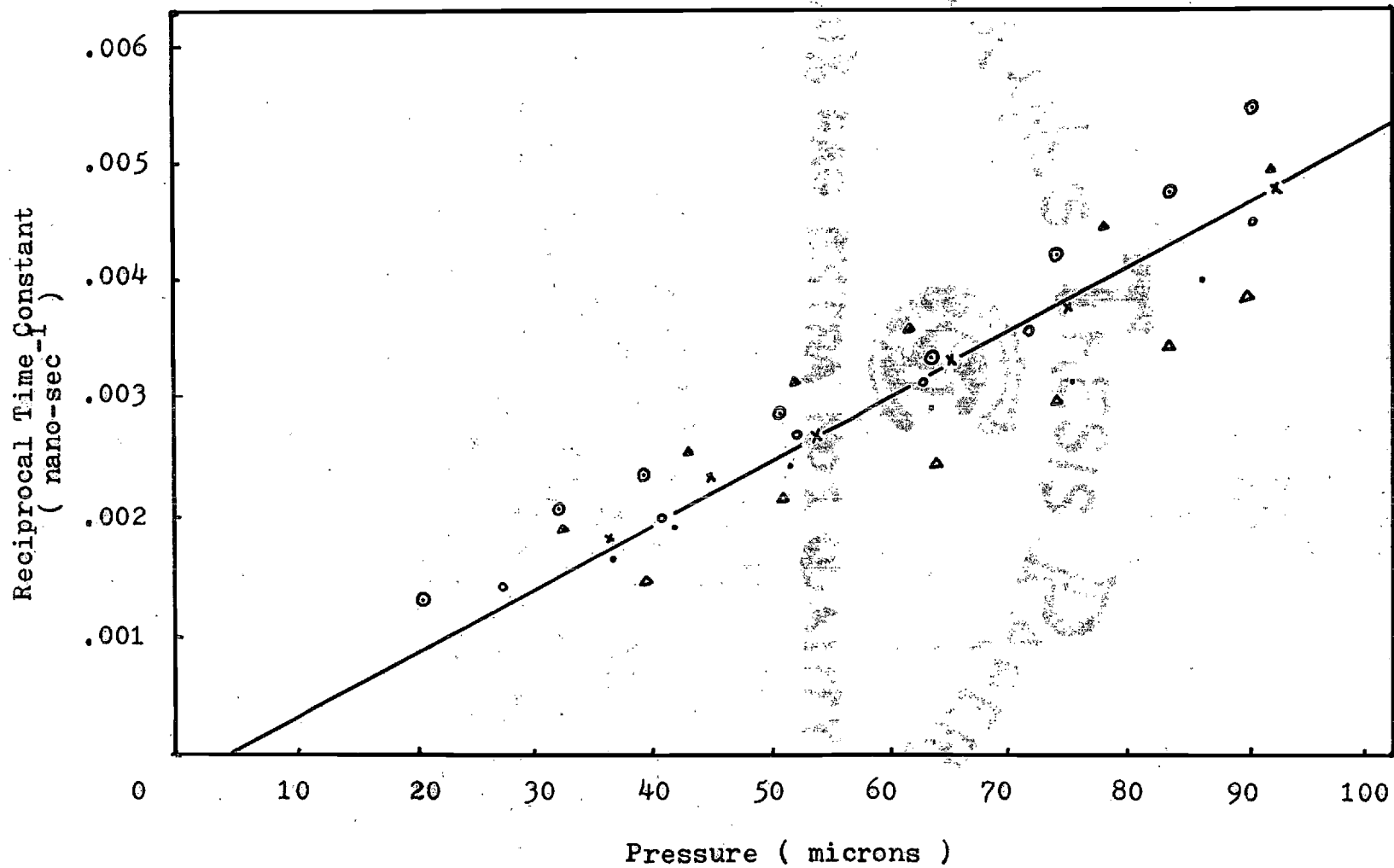


Figure 26. Results of Six Sets of Measurement of Time Constant and Pressure of OCS  $J = 2 \rightarrow 1$ ,  $V = 0$ .

shows the results of 5 different measurements. The original data are given in Appendix C. All these measurements were taken at different times under what were supposed to be the same physical conditions. As seen from figure 26 the slopes obtained on different runs are not changed appreciably which implies that the line-breadth parameter  $\Delta\nu_p$  will still check with the theoretical prediction. As will be discussed in the next section, one of the possible factors which might have influenced these measurements is the temperature.

The other sample gas chosen for this investigation was ammonia. The results of the measurement are shown in Figure 27. A 1087 volts/cm Stark field was applied to the electrode inside the absorption cell where the sample gas was stored and the gas was cooled to dry ice temperature. The klystron frequency was locked at 23878.04 MHz, 8.03 MHz above the  $\text{NH}_3$  inversion line. The data are shown in Table 2 and plotted in Figure 27. The slope of the curve on Figure 27 was found to be  $2.3 \times 10^{-5}$  cycle/(n-sec) (micron). After considering the temperature correction, changing the units and applying  $\Delta\nu = \frac{1}{2\pi\tau}$  the line-broadening parameter was found to be 2.4 Mc/mm-Hg which is about ten times smaller than line-broadening experiment results, i.e., 24 Mc/mm-Hg reported by Legan, Roberts, Rinehart and Lin (10). This measurement of time constant as a function of pressure was repeated more than ten times with great precautions. Some of the results are shown in Figure 28 with data reported in Appendix C. As can

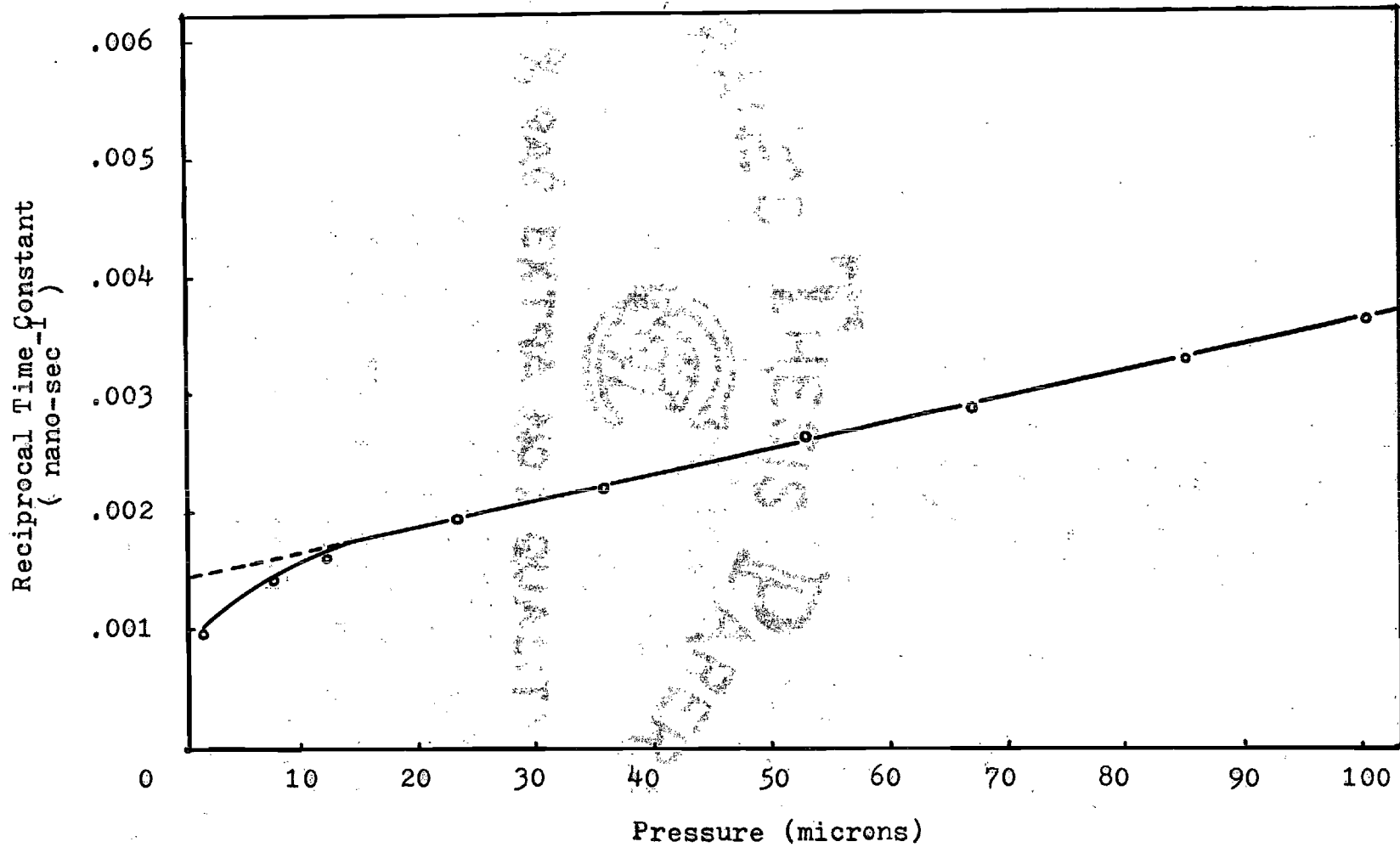


Figure 27. Reciprocal Time Constants versus Pressure,  $\text{NH}_3$  (3,3).

Table 2. Pressure, Signal Amplitude and  
Time Constant for  $\text{NH}_3$

Pressure (Micron)	Signal Amplitude (Millivolt)	Time Constant (Nano-sec)	Reciprocal Time Constant (Nano-sec <sup>-1</sup> )
100.9	9.0	255	0.00392
85.2	10.0	303	0.00330
66.9	11.5	341	0.00293
52.8	13.0	373	0.00268
36.0	14.5	450	0.00222
23.1	16.0	507	0.00197
11.9	17.5	610	0.00164
6.9	17.0	736	0.00136
2.2	15.5	915	0.00107

AND EXTRA TO QUALITY

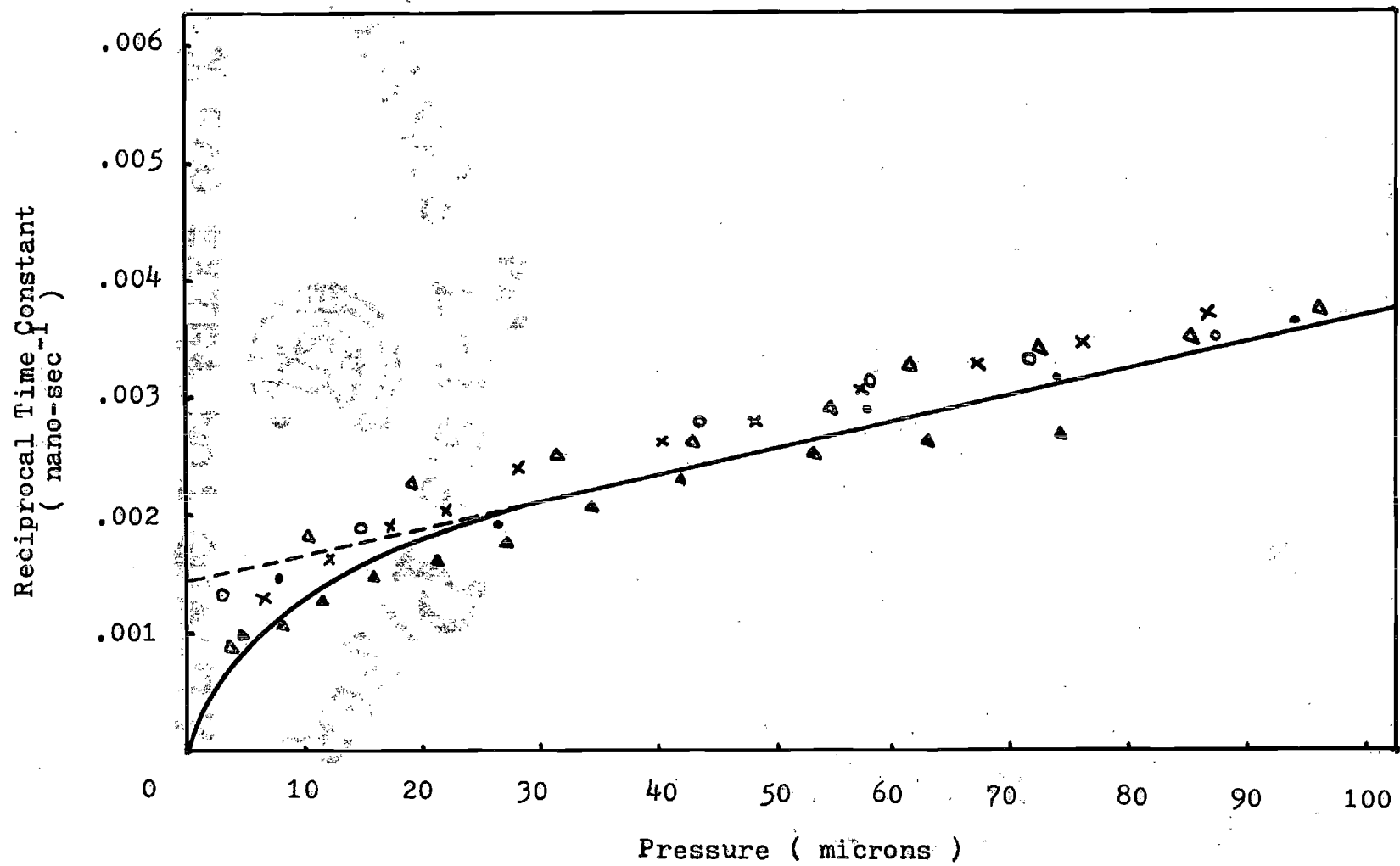


Figure 28. Results of Five Sets of Measurement of Time Constant and Pressure of  $\text{NH}_3$  (3,3).

be seen from Figure 28, even though the data are scattered the slope of the curve on each performance is close to the value shown in Figure 27, i.e.,  $2.30 \times 10^{-5}$  cycle/(n-sec) (micron).

### Temperature

Over the pressure range in which line broadening is directly proportional to pressure,  $\Delta\nu$  can be expressed (11) as

$$\frac{\Delta\nu}{\Delta\nu_s} = \left(\frac{T}{300}\right)^x \quad (15)$$

where  $\Delta\nu_s$  is the line breadth at room temperature and at the same pressure as  $\Delta\nu$ .  $T$  is the absolute temperature at which  $\Delta\nu$  is measured. There is some uncertainty about the temperature dependence of the line breadth, i.e., the value of  $x$ . On the theoretical part, Anderson (12) and Margenau (13) have predicted that the collision cross section should vary inversely with temperature, giving  $x = -1$ . Experimentally, Johnson and Slager (14) have found the rotational lines of OCS to vary in width approximately as  $T^{-3/2}$ . Beiviger and Castle (15) observed that the width of the paramagnetic resonance lines of  $O_2$  varied as  $T^{-3/4}$ . The measurements of Hill and Gordy (16) on several lines indicated a variation as  $T^{-1}$  approximately.

In order to find the influence of temperature on the decay rate observed here two measurements were made under

the same physical conditions except that one was made with dry ice on the absorption cell and the other without. Both of these measurements were performed with ammonia gas as sample with the same power level, the same Stark field (1087 volts/cm), the same klystron frequency (8.01 MHz above  $\text{NH}_3$  inversion line) and the same pressure range (8 to 93 micron-Hg). The data are reported in Table 6 in Appendix C and the results are shown in Figure 29.

In order to compare the results of this investigation with other known values, equation (15) will be rewritten using  $\Delta\nu = (2\pi\tau)^{-1}$ . Hence X becomes

$$X = \frac{\log\left(\frac{\tau_s}{\tau}\right)}{\log\left(\frac{T}{300}\right)}. \quad (16)$$

The measurements were made at room temperature and at dry ice temperature therefore  $T = 195^\circ\text{K}$  in equation (16). From Figure 29, for a certain fixed value of pressure the ratio  $\tau_s/\tau$  can be found and therefore a value of X can be calculated. The result is shown in Table 3.

From Table 3 one can see that the value of X is slightly reduced as the pressure goes down, therefore equation (15) does not predict the observed temperature dependence of  $\tau$  exactly. The average value of X from Table 3 is -0.650 which is approximately Johnson and Slager's value

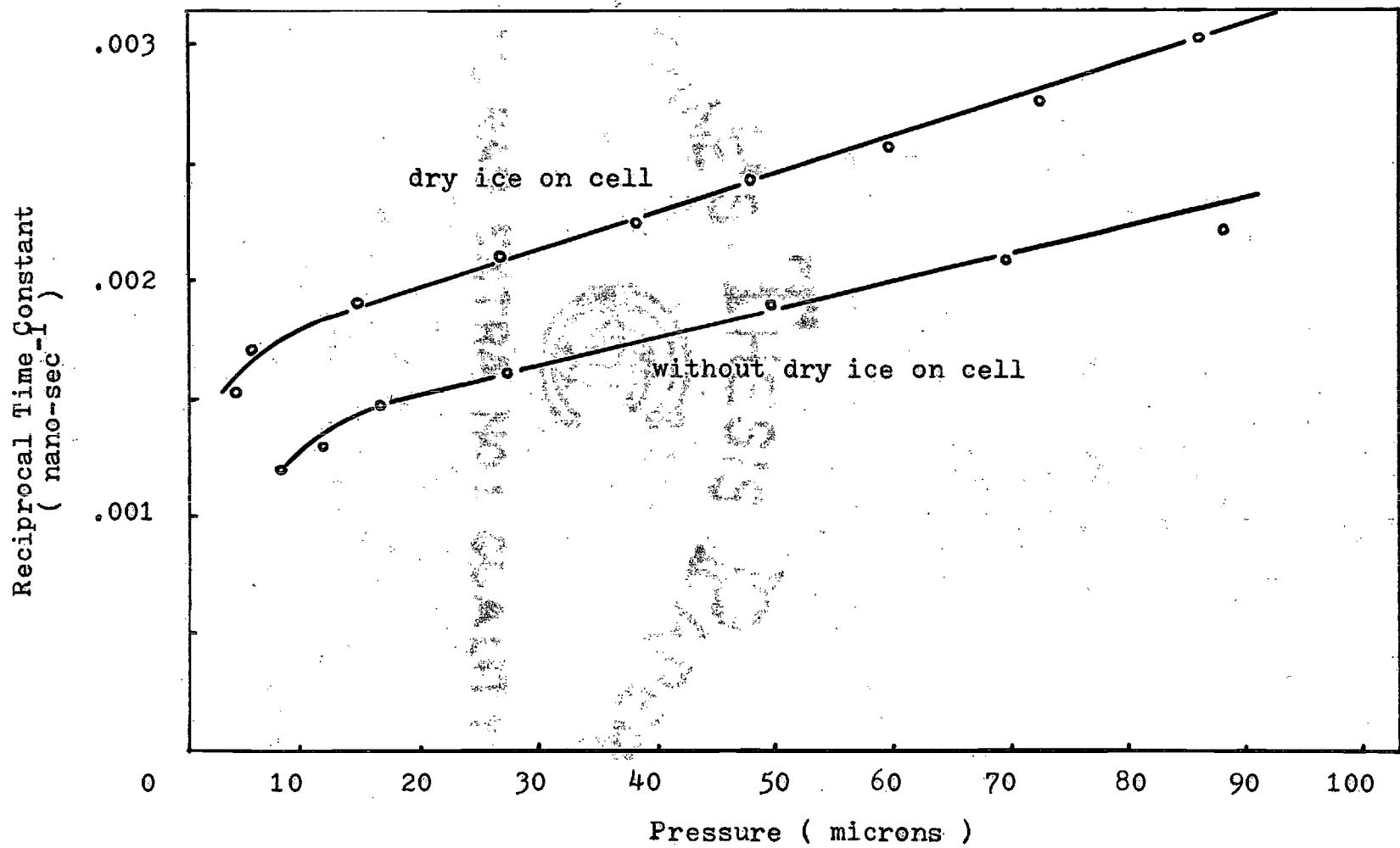


Figure 29. Relationship of Time Constant and Temperature,  $\text{NH}_3$  (3,3).

Table 3. Pressure and Temperature Factor X

Pressure (Micron)	$\tau_s/\tau$	X
90	1.345	-0.668
80	1.341	-0.681
70	1.340	-0.679
60	1.330	-0.662
50	1.320	-0.644
40	1.314	-0.634
30	1.299	-0.607
20	1.296	-0.602

-0.667.

### Power

As was discussed in Chapter II and observed in the last section the klystron power is not a critical factor as far as observing the signal is concerned. In addition, no noticeable change of decay rate could be detected for a fairly large range of power levels (between 4 and 20 db of the attenuation). The signal amplitude, on the other hand is changed with klystron power level, as indicated by Figure 20. Hence the main reason for setting the variable attenuator at 11.5 db was to give the optimum beat signal and maximum signal amplitude.

### The Relation Between Signal Amplitude and Other Physical Parameters

Throughout this study it was found that the signal amplitude, the height of the second positive peak above the center line as shown on Figure 16(b), varied when environmental conditions changed. These conditions included pressure, temperature and klystron power passing through the sample gas. Theoretically, the larger signal amplitude indicates that more sample molecules are radiating in phase during the emission process.

### Pressure

Both  $\text{NH}_3$  and OCS were used for this study. The sample gas was cooled to dry ice temperature for the purpose of in-

creasing the signal amplitude and hence increasing the accuracy of the amplitude measurement. The klystron power level was adjusted to the optimum value at the start of each run. The  $\text{NH}_3$  molecules were introduced under a Stark field of about 1087 volts/cm and the klystron was locked at 8 MHz above the inversion line. The OCS molecules were under 3265 volts/cm Stark field and the klystron was stabilized at 5 MHz above the rotational line.

The results are tabulated in Tables 1 and 2, and also plotted in Figure 30. As can be seen from Figure 30 both sample gases show a maximum in signal amplitude as the pressure is reduced. This phenomenon can be explained as follows. Before the signal reaches its maximum, i.e., at a higher pressure, the probability that the molecules will radiate in phase is small due to the large interaction between molecules, therefore the signal is smaller. As the pressure goes down, the chance that the molecules will radiate in phase becomes larger and larger and this increases the amplitude. However as the pressure is reduced the number of molecules radiating decreases. Therefore, a point is reached where the amplitude goes through a maximum, and then decreases as the pressure is further reduced.

#### Temperature

In order to see the influence of temperature on the signal amplitude, ammonia gas was admitted to the absorption cell without dry ice on the waveguide. The pressure versus

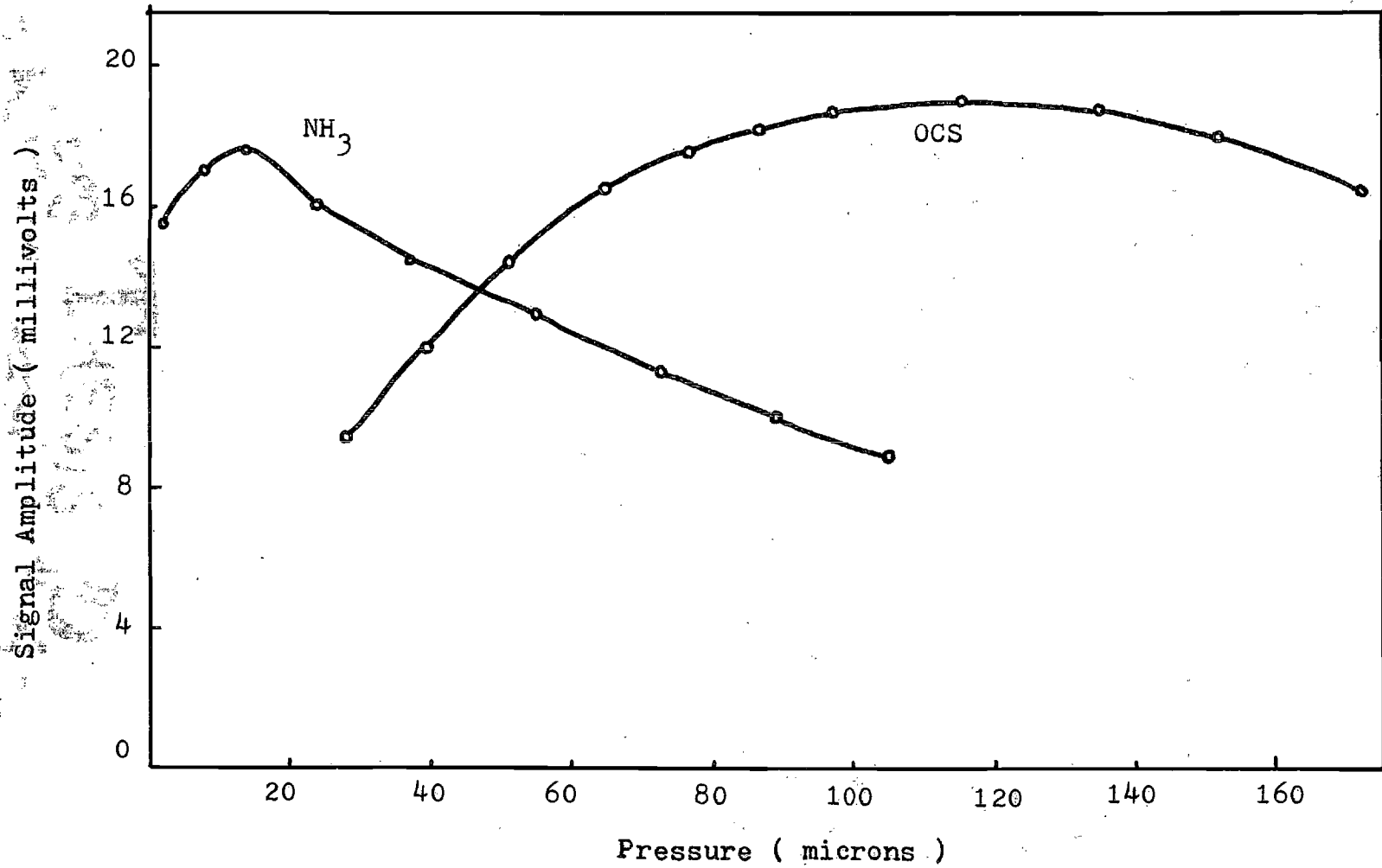


Figure 30. Signal Amplitude and Pressure Relation

signal amplitude measurement was performed under the same conditions as when the absorption cell was surrounded by dry ice. The data are shown in Table 7 of Appendix C and plotted in Figure 31. The figure shows that the signal amplitude is much smaller at room temperature as expected. The primary reason for the amplitude being larger at the lower temperature is the fact that the ammonia (3,3) inversion line is a low-J transition and therefore the initial state for the transition is more highly populated at the lower temperature.

#### Klystron Power

To study the change of signal amplitude as the klystron power is changed, the ammonia gas was chosen as sample. The pressure inside the absorption cell was 14 micron-Hg and temperature was  $-80^{\circ}\text{C}$ . The klystron was locked at 23878.12 MHz by the lock-in system described in Chapter III. The klystron power was varied by adjusting the calibrated variable attenuator in front of the absorption cell. The crystal current at the detector was read by a Triplitt 630-APLK meter. The power was read from a crystal current versus power chart which was obtained earlier using a Hewlett-Packard power meter. The results are shown in Table 8, Appendix C and in Figure 32. Figure 32 shows that when the klystron power was high, such as 5.0 milliwatts, the beat signal was saturated and distorted as shown in Figure 20 part (a). Therefore the reading of the signal amplitude, from the center line to the top of the second positive peak was

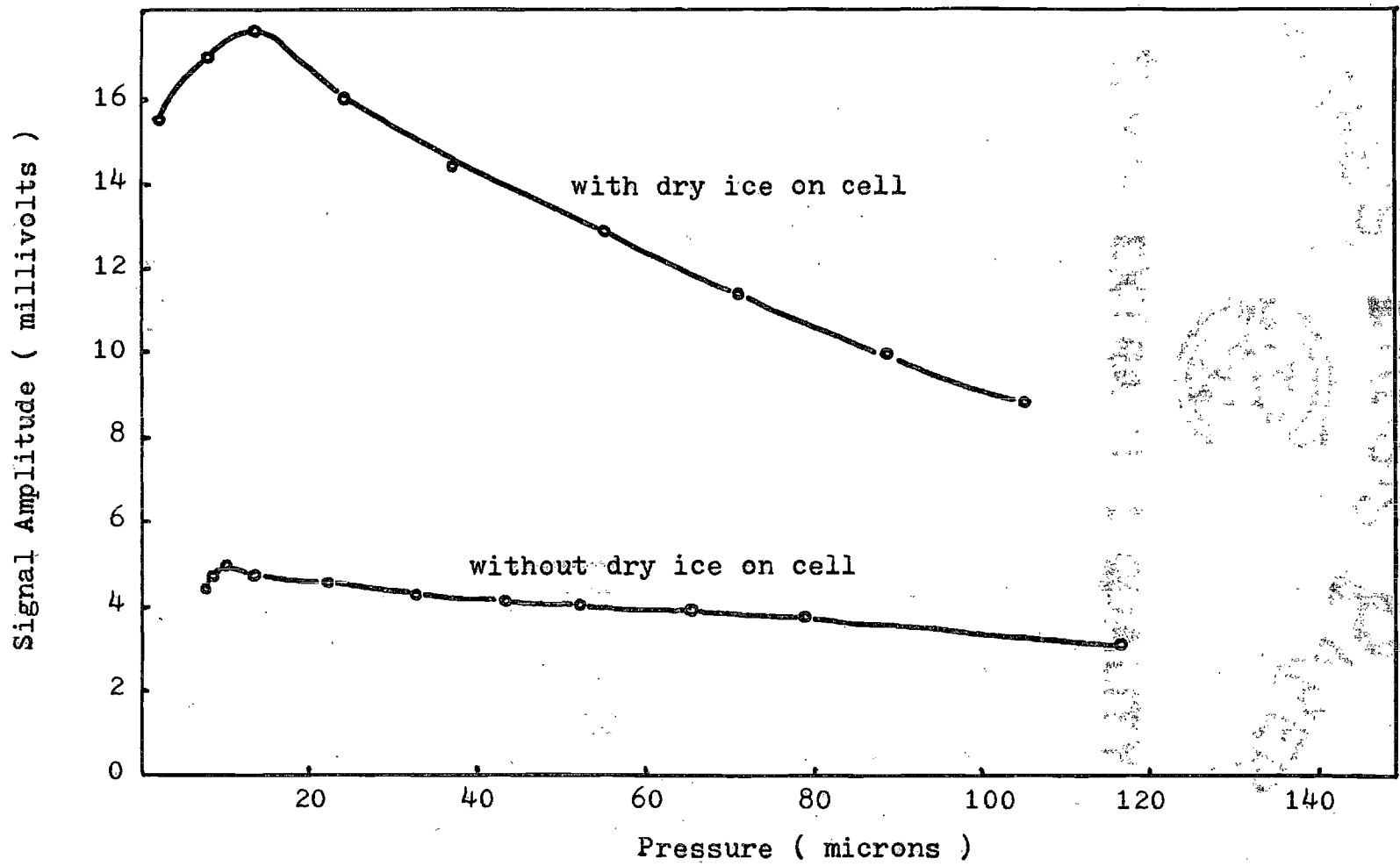


Figure 31. Signal Amplitude and Temperature Relation

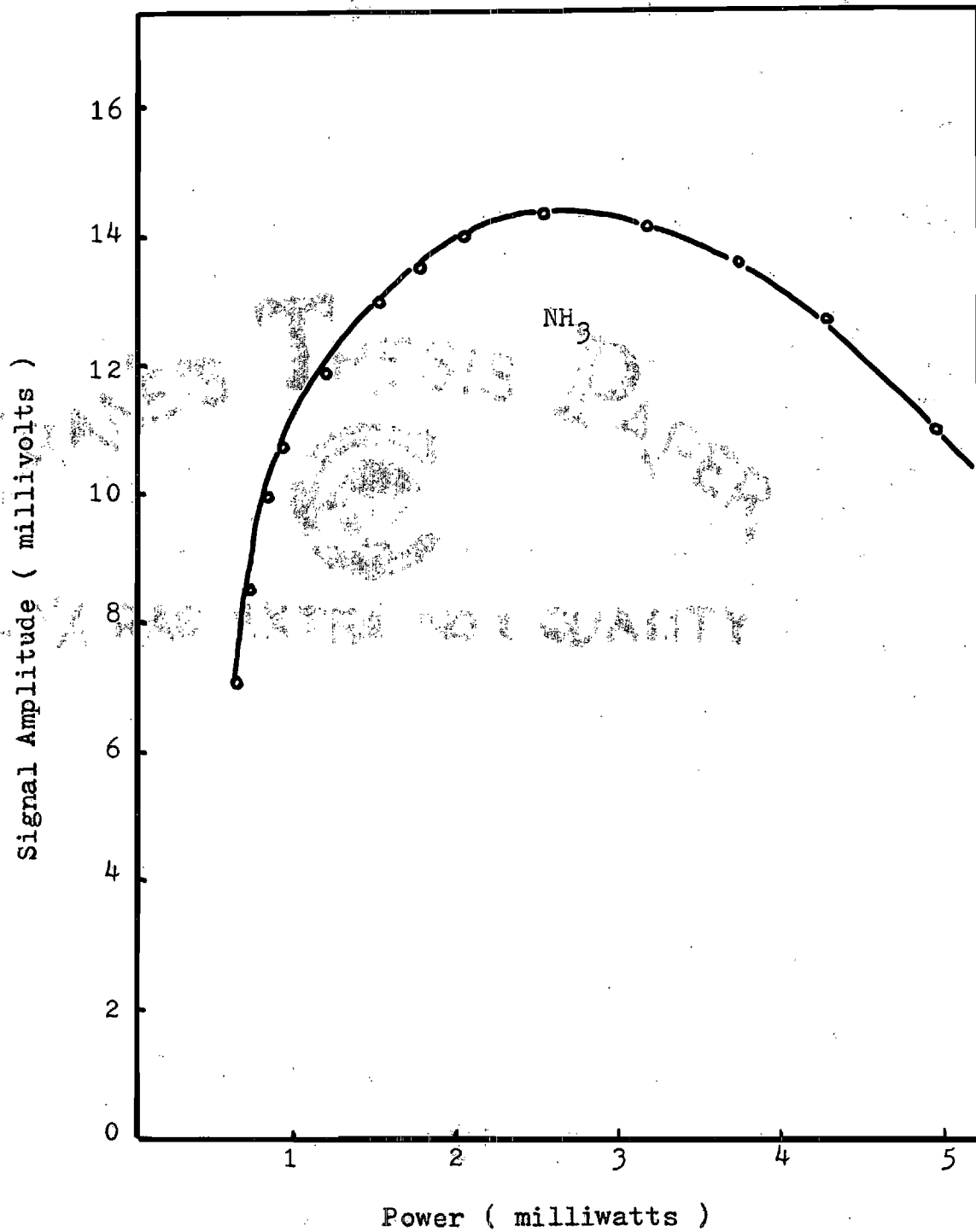


Figure 32. Signal Amplitude and Klystron Power Relation.

smaller in this region. As the klystron power was reduced it passed through a broad range of stable signal amplitudes including the optimum value at 2.5 milliwatts. As the klystron power was further reduced below 2 milliwatts the amplitude was drastically reduced.

### The Emission Radiation Power

One of the interests of this investigation was to measure the amount of microwave power emitted during the molecules radiation process. Because the radiated power was so small a careful indirect measurement was needed. A schematic diagram of the apparatus used is shown in Figure 33.

The ammonia gas at a pressure of about 30 micron-Hg was introduced to the absorption cell which was cooled with dry ice. Klystron number one was the main microwave source, and its frequency was locked at 8 MHz above the  $\text{NH}_3$  (3,3) inversion line by the lock-in unit described in Chapter III. The Stark component was swept through the klystron frequency by the applied Stark field and the beat between the molecular radiation and the klystron radiation was detected by the signal detection unit also described in Chapter III. Between the absorption cell and detection unit a directional coupler was connected in order to add in a microwave line consisting of a second klystron, an isolator, a wavemeter and two calibrated variable attenuators.

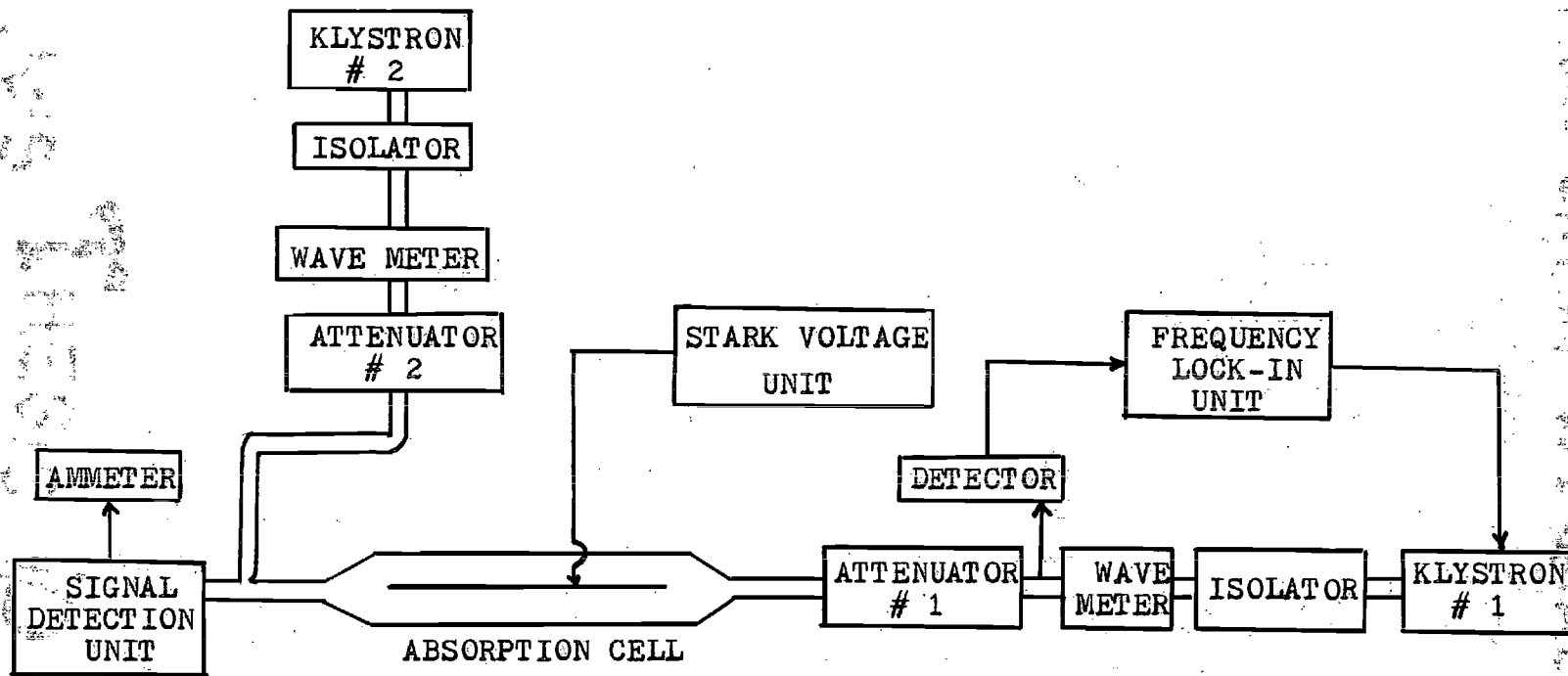


Figure 33. Block Diagram of Apparatus Used for the Radiation Power Measurement.

Klystron 2 was tuned to the ammonia line frequency, and its power was measured at the detector with a known setting of attenuator 2. Then attenuator 2 was adjusted until the amplitude of the beat between the radiations of klystrons 1 and 2 matched the beat amplitude between the molecular radiation and the radiation of klystron 1. Knowing the settings of attenuator 2 in both of the above cases one can calculate the power from klystron 2 required to produce a beat of the same amplitude as the molecular radiation beat signal. This klystron 2 power should be equal to the molecular radiation power. From this measurement the molecular radiation power was found to be approximately  $0.024 \pm .003 \mu\text{w}$ .

## CHAPTER V

## CONCLUSIONS AND RECOMMENDATIONS

The results of this investigation have shown that the adiabatic rapid passage technique can be used to excite gas molecules. It has also been demonstrated that the molecular radiation occurring after excitation is coherent. This is evident from the fact that a clear beat signal is produced when the molecular radiation and the klystron radiation fall on the detector.

The most surprising result of this investigation has been that the decay time for the molecular radiation in the case of ammonia is about ten times longer than that which would be expected from direct line width measurements. This seems to indicate that not all of the collisions which contribute to broadening of the ammonia line interrupt the coherent radiation process observed in this experiment. The measured decay rate of the OCS  $J = 2 \rightarrow 1$  transition, on the other hand, is just slightly larger than that calculated from the line broadening parameter. Macke and Glorieux (17) observed a much slower decay rate for OCS but Hill et al (18) reported a result similar to that obtained in this investigation. An extension of this investigation to other gas molecules is recommended, in the hope of finding an explana-

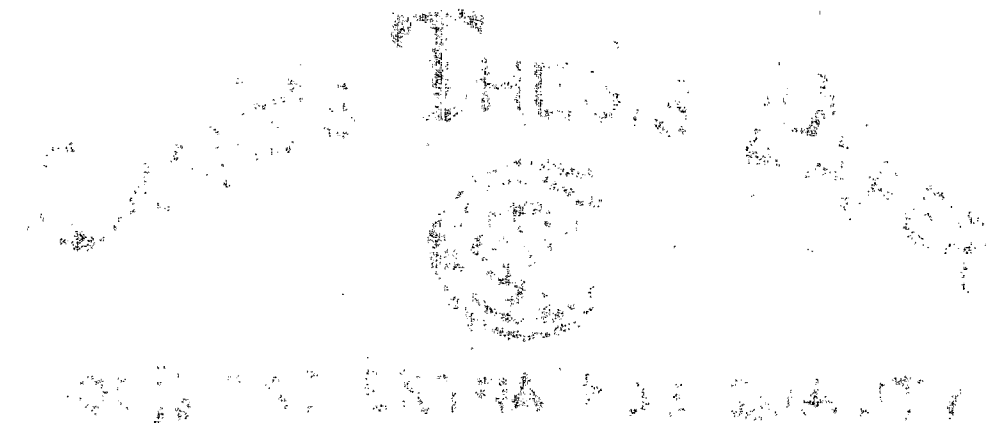
tion of the contradictory results for the decay times for  $\text{NH}_3$  and OCS.

The beat signal, between the molecular radiation and the klystron radiation, was studied under different pressures, temperatures and klystron power levels. It was found that the decay rate of the beat signal is inversely proportional to the pressure and remains constant for a fairly wide range of klystron power levels. The relation between temperature and decay rate is not given exactly by the simple equation suggested by Gordy et al (19).

The relations between signal amplitude and pressure, temperature, and klystron power have also been studied. It was found that both  $\text{NH}_3$  and OCS signal amplitudes pass through a maximum as the pressure changes. At very low pressure, below 40 microns, the signal amplitude of  $\text{NH}_3$  is much larger than that of the OCS and this is consistent with the fact that the line intensity of  $\text{NH}_3$  is about ten times larger than that of OCS. Above 50 microns the  $\text{NH}_3$  signal amplitude is smaller than that of OCS because the  $\text{NH}_3$  molecule has a larger dipole moment which perturbs the neighboring molecules. This causes the  $\text{NH}_3$  molecules to radiate at slightly different frequencies and coherence is lost. It was also found that the signal amplitude increased as temperature decreased as one would expect for a low-J transition. The signal amplitude passes through a broad maximum as the klystron power level changes.

The molecular radiation power was estimated to be  $0.024 \pm 0.003$  microwatts for the first 100 nano-seconds of the radiation.

Since the rate of sweep and the klystron power are not critical so long as they fall within some broad limits, and since only a low power is required this method of exciting molecules should be a useful tool in other experiments. For example, it should be possible to use adiabatic rapid passage as the method of excitation in performing microwave double-resonance experiments (20) and in observing the collisional transfer of rotational energy (21).



APPENDIX A

THE DERIVATION OF THE SOLUTIONS OF EQUATION (10)

THE DERIVATION OF THE SOLUTIONS OF EQUATION (10)

The derivation of solutions of equation (10) can be traced as follows: Consider two non-degenerate states, namely ground state  $g$  and excited state  $e$ , interacting by Hamiltonian

$$\begin{aligned} H' &= -\vec{\mu} \cdot \vec{E} = -\mu_x E_x = -\mu_x 2E_x^0 \cos 2\pi\nu t \\ &= -\mu_x E_x^0 (e^{2\pi i\nu t} + e^{-2\pi i\nu t}) \end{aligned} \quad (A1)$$

where  $2E_x^0$  is the amplitude of the radiation E-field. The time-dependent coefficient of the ground state component of the wavefunction will be

$$\dot{a}_g(t) = -\frac{2\pi i}{h} a_g \int \psi_g^{0*} H' \psi_g^0 dt - \frac{2\pi i}{h} a_e \int \psi_g^0 H' \psi_e^{0*} dt \quad (A2)$$

Expanding term  $\psi_g^0$  by  $\psi_g^0 \exp\left[-(2\pi i E_g^0 t/h)\right]$  and from  $\int \psi_g^0 \mu_x \psi_g^{0*} dt = 0$  the upper equation can be written as

$$\begin{aligned} \dot{a}_g(t) &= \frac{2\pi i}{h} a_e E_x^0 \mu_{xge} \left\{ \exp\left[\frac{-2\pi i t}{h} (E_e^0 - E_g^0 - h\nu)\right] \right. \\ &\quad \left. + \exp\left[\frac{-2\pi i t}{h} (E_e^0 - E_g^0 + h\nu)\right] \right\} \end{aligned} \quad (A3)$$

where  $\mu_{xge}$  is the matrix element of dipole moment  $\mu_x$  linking states  $g$  and  $e$ . Ignoring the rapidly varying term  $\exp\left\{-2\pi i (E_e^0 - E_g^0 + h\nu) t/h\right\}$  and letting

$$\mu_{xge} = \left| \mu_{xeg} \right| e^{-i\alpha}, \quad C = \frac{2\pi}{h} E_x^0 \left| \mu_{xeg} \right|,$$

$$\omega_R = \frac{2\pi}{h} (E_e^0 - E_g^0), \quad \omega = 2\pi\nu$$

then one obtains

$$\dot{a}_g(t) = i C a_e \exp\left[-i(\omega_R - \omega)t - i\alpha\right]. \quad (A4)$$

Similarly, it can be shown that

$$\dot{a}_e(t) = i C a_g \exp\left[i(\omega_R - \omega)t + i\alpha\right]. \quad (A5)$$

By taking the second derivative of equation (A5) it can be shown that

$$\ddot{a}_e(t) - i(\omega_R - \omega)\dot{a}_e(t) + C^2 a_e(t) = 0. \quad (A6)$$

In order to simplify the notation let

$$n = (m^2 + C^2)^{\frac{1}{2}}, \quad m = -\frac{1}{2}(\omega_R - \omega)$$

and equation (A6) becomes

$$\ddot{a}_e(t) - i2m \dot{a}_e(t) + (n^2 - m^2) a_e(t) = 0 . \quad (\text{A7})$$

Solving the differential equation (A7) by using two integration constants,  $c_1$  and  $c_2$ , it is found that

$$a_e(t) = \exp(-imt) \left[ -\frac{ic_1}{2n} \exp(int) + c_2 \exp(-int) \right] . \quad (\text{A8})$$

Similarly one finds

$$a_g(t) = \frac{-1}{c} \exp(int - i\alpha) \left[ \frac{ic_1}{2n} (n-m) \exp(int) + c_2 (n+m) \exp(-int) \right] . \quad (\text{A9})$$

In order to eliminate the integration constants consider the special case when  $t = 0$ , i.e.,

$$a_e(0) = \frac{-ic_1}{2n} + c_2 = a_{oe} \quad (\text{A10})$$

$$a_g(0) = \left[ \frac{-i(n-m)}{2mn} c_1 - \frac{(n+m)}{c} c_2 \right] e^{-i\alpha} = a_{og}$$

and solving equation (A10) for  $c_1$  and  $c_2$  gives

$$c_1 = ic a_{og} e^{i\alpha} + i(m+n) a_{oe}$$

and

$$c_2 = -\frac{c}{2n} e^{i\alpha} a_{og} + \frac{(n-m)}{2n} a_{oe} . \quad (\text{A11})$$

Substituting equation (A11) into equation (A8) and (A9) and expressing the time-dependent exponentials in terms of sines and cosines one obtains

$$a_e(t) = \left[ \exp(-imt) \right] \left[ a_{oe} \left( \cos nt + \frac{im}{n} \sin nt \right) + \frac{ic}{n} e^{i\alpha} (\sin nt) a_{og} \right] . \quad (\text{A12})$$

$$a_g(t) = \left[ \exp(imt) \right] \left[ \frac{ic}{n} e^{-i\alpha} a_{oe} \sin nt + a_{og} \left( \cos nt - \frac{im}{n} \sin nt \right) \right] . \quad (\text{A13})$$

when  $\omega = \omega_R$ , i.e., the sweep frequency is fixed at the resonance frequency then  $m = 0$  and equation (A12) and equation (A13) become

$$a_e(t) = a_{oe} \cos ct + i e^{i\alpha} a_{og} \sin ct$$

(A14)

and

$$a_g(t) = a_{og} \cos ct + i e^{-i\alpha} a_{oe} \sin ct .$$

For the case in which the system is initially in the ground state,  $a_{og} = 1$  and  $a_{oe} = 0$ , and one obtains

$$a_e(t) = i e^{i\alpha} \sin ct, \quad a_g(t) = \cos ct. \quad (A15)$$

The probabilities of the system being in ground and excited states are

$$a_e^*(t) a_e(t) = \sin^2 ct, \quad a_g^*(t) a_g(t) = \cos^2 ct. \quad (A16)$$

This is the result plotted in Figure 4.

APPENDIX B  
COMPUTER CALCULATION  
OF THE POPULATION PROBABILITY



COMPUTER CALCULATION  
OF THE POPULATION PROBABILITY

For an infinitesimal time interval  $\Delta t$  the increment of the coefficient of the wavefunction can be written as

$$a_g(t + \Delta t) \doteq a_g(t) + \dot{a}_g(t)\Delta t. \quad (B1)$$

From equation (A4) of Appendix A it is found that

$$a_g(t + \Delta t) \doteq a_g(t) + i c a_e(t) \exp[i(\omega_R - \omega)t] \Delta t. \quad (B2)$$

Let  $\omega = \omega_R + kt$ , and equation (B2) becomes

$$a_g(t + \Delta t) \doteq a_g(t) + i c a_e(t) \exp[+ikt^2] \Delta t. \quad (B3)$$

Suppose that  $\omega$  changes from  $\omega_R - \Delta\omega$  to  $\omega_R + \Delta\omega$  while the time goes from  $-T$  to  $+T$  as indicated below

$\omega \longrightarrow$	$\omega_R - \Delta\omega$	$\omega_R$	$\omega_R + \Delta\omega$
$t \longrightarrow$	$-T$	$0$	$+T$

Then  $\Delta\omega = kT$  of  $k = \Delta\omega/T$ . If the interval from  $t = -T$  to  $t = T$  is divided into  $2N$  steps of magnitude  $\Delta t = \frac{T}{N}$  and the

steps are numbered  $I = 0, 1, 2, \dots, 2N$  then equation (B3) can be written

$$a_g(I+1) = a_g(I) + \frac{icT}{N} a_e(I) \exp\left\{+ik\left(\frac{I-N}{N}T\right)^2\right\}. \quad (B4)$$

Since the values of  $a_g(I)$  and  $a_e(I)$  are complex numbers, by using the superscripts  $r$  and  $i$  to represent real and imaginary parts respectively, equation (B4) becomes

$$\begin{aligned} a_g^r(I+1) + ia_g^i(I+1) &= a_g^r(I) + ia_g^i(I) \\ &+ i\frac{cT}{N} \left\{ a_e^r(I) + ia_e^i(I) \right\} \left( \cos B + i \sin B \right). \end{aligned} \quad (B5)$$

where  $B = k\left(\frac{I-N}{N}T\right)^2$ . Collecting real and imaginary parts, separately from equation (B5) it becomes four equations, namely,

$$\begin{aligned} a_g^r(I+1) &= a_g^r(I) + \frac{cT}{N} \left\{ a_e^r \sin B - a_e^i \cos B \right\} \\ a_g^i(I+1) &= a_g^i(I) + \frac{cT}{N} \left\{ a_e^i \sin B + a_e^r \cos B \right\} \\ a_e^r(I+1) &= a_e^r(I) + \frac{cT}{N} \left\{ -a_g^r \sin B - a_g^i \cos B \right\} \\ a_e^i(I+1) &= a_e^i(I) + \frac{cT}{N} \left\{ -a_g^i \sin B + a_g^r \cos B \right\}. \end{aligned} \quad (B6)$$

A Focal computer language was applied to write the equation (B6) into the computer program. A typical program and a portion of the results is shown on the next page.

\*W

C:FOCAL-11,PRELIM

2.20 S C(1)=40\*10<sup>6</sup> ; S C(2)=100\*10<sup>6</sup>; S C(3)=500\*10<sup>6</sup>; S NO=1  
 2.40 S N=10000; S L=4/10<sup>7</sup> ; S K=10<sup>15</sup>  
 2.70 F V=1,1,N0; S M1=0; S M2=0; S N1=1; S N2=0; D 2.8  
 2.75 QUIT  
 2.80 S E=C(V)\*L/N ; D 2.9 ; D 2.91; F I=0,1,2\*N ; D 3  
 2.90 T %10,!!,"C(V)",C(V); T %4.4," E",E; T %7," N",N,!!  
 2.91 T " I"," M+2", " N+2"," M+2+N+2",!

3.10 S J=[M1+2+M2+2] ; S Q=[N1+2+N2+2]  
 3.12 IF [I/40-FITR(I/40)]3.20,3.15,3.20  
 3.15 T %4,I/10; T %4.03,J ; T %4.03,Q,J+Q,!  
 3.20 S B=K\*[(I-N)\*L/N]<sup>2</sup>  
 3.30 S J1=M1+E\*[-N2\*FCOS(B)+N1\*FSIN(B)]  
 3.35 S J2=M2+E\*[N1\*FCOS(B)+N2\*FSIN(B)]  
 3.40 S Q1=N1-E\*[M2\*FCOS(B)+M1\*FSIN(B)]  
 3.45 S Q2=N2+E\*[M1\*FCOS(B)-M2\*FSIN(B)]  
 3.90 S M1=J1 ; S M2=J2 ; S N1=Q1 ; S N2=Q2

\*G

C(V)= 40000000 E= 0.002 N= 10000

I	M+2	N+2	M+2+N+2
= 0=	0.000	= 1.000	= 1.000
= 4=	0.004	= 0.997	= 1.000
= 8=	0.009	= 0.991	= 1.000
= 12=	0.009	= 0.991	= 1.000
= 16=	0.003	= 0.997	= 1.000
= 20=	0.000	= 1.000	= 1.000
= 24=	0.004	= 0.997	= 1.001
= 28=	0.009	= 0.991	= 1.001
= 32=	0.009	= 0.992	= 1.001
= 36=	0.003	= 0.998	= 1.001
= 40=	0.000	= 1.001	= 1.001
= 44=	0.004	= 0.997	= 1.001
= 48=	0.009	= 0.992	= 1.001
= 52=	0.010	= 0.992	= 1.001
= 56=	0.004	= 0.997	= 1.001
= 60=	0.000	= 1.001	= 1.001
= 64=	0.003	= 0.999	= 1.002
= 68=	0.009	= 0.993	= 1.002
= 72=	0.010	= 0.991	= 1.002
= 76=	0.006	= 0.996	= 1.002
= 80=	0.000	= 1.001	= 1.002
= 84=	0.002	= 1.001	= 1.002

APPENDIX C  
TABLES OF TIME CONSTANT AND PRESSURE,  
TEMPERATURE RELATION MEASUREMENT

## TABLES OF TIME CONSTANT AND PRESSURE

## TEMPERATURE RELATION MEASUREMENT

Table 4. OCS Data of Figure 26

Pressure (Micron)	Time Constant (Nano-sec)	Reciprocal Time Constant, (Nano-sec <sup>-1</sup> )	Designation
106.0	182	0.00549	X
93.0	210	0.00476	
75.5	265	0.00377	
65.5	300	0.00333	
54.0	376	0.00266	
45.0	430	0.00233	
36.5	554	0.00181	
116.5	173	0.00578	
101.0	189	0.00529	
86.5	250	0.00400	
76.0	317	0.00315	
64.0	342	0.00292	
52.0	415	0.00241	
42.0	526	0.00190	

( Continued )

Table 4. OCS Data of Figure 26

Pressure (Micron)	Time Constant (Nano-sec)	Reciprocal Time Constant (Nano-sec <sup>-1</sup> )	Designation
91.0	182	0.00549	⊙
84.0	210	0.00476	
74.5	237	0.00422	
64.2	300	0.00333	
51.0	348	0.00287	
39.5	425	0.00235	
32.2	486	0.00206	
20.6	750	0.00133	
143.0	127	0.00787	▲
118.0	140	0.00714	
92.5	163	0.00613	
78.5	183	0.00546	
62.0	202	0.00495	
52.0	220	0.00455	
43.5	278	0.00360	
32.5	362	0.00276	

( Continued )

Table 4. OCS Data of Figure 26

Pressure (Micron)	Time Constant (Nano-sec)	Reciprocal Time Constant (Nano-sec <sup>-1</sup> )	Designation
190.7	107	0.00935	
161.8	120	0.00833	
121.5	135	0.00741	
91.2	222	0.00450	
72.2	279	0.00358	
63.8	320	0.00312	
52.7	370	0.00270	
41.4	500	0.00200	
27.7	670	0.00149	

Table 5.  $\text{NH}_3$  Data of Figure 28

Pressure (Micron)	Time Constant (Nano-sec)	Reciprocal Time Constant <sub>1</sub> (Nano-sec <sup>-1</sup> )	Designation
104.0	267	0.00375	●
89.8	287	0.00348	
70.1	330	0.00303	
54.6	363	0.00275	
47.9	405	0.00247	
35.4	485	0.00215	
25.0	550	0.00182	
15.4	625	0.00160	
7.6	727	0.00138	
1.8	850	0.00118	
105.7	250	0.00400	●
82.7	300	0.00333	
67.6	315	0.00317	
54.8	335	0.00299	
40.8	375	0.00267	
14.0	565	0.00177	
2.8	840	0.00122	

( continued )

Table 5. NH<sub>3</sub> Data of Figure 28

Pressure (Micron)	Time Constant (Nano-sec)	Reciprocal Time Constant (Nano-sec <sup>-1</sup> )	Designation
89.5	280	0.00357	△
80.5	300	0.00333	
68.5	310	0.00322	
58.0	320	0.00312	
50.5	360	0.00278	
40.5	400	0.00250	
29.5	420	0.00238	
24.0	440	0.00227	
18.0	460	0.00217	
13.0	540	0.00185	
10.0	580	0.00172	
5.4	960	0.00103	

( continued )

Table 5. NH<sub>3</sub> Data of Figure 28

Pressure (Micron)	Time Constant (Nano-sec)	Reciprocal Time Constant (Nano-sec <sup>-1</sup> )	Designation
82.0	280	0.00357	×
72.0	300	0.00333	
63.5	320	0.00312	
53.0	340	0.00294	
45.2	380	0.00263	
38.0	400	0.00250	
26.5	440	0.00227	
20.5	520	0.00192	
16.5	560	0.00179	
11.3	640	0.00156	
6.5	840	0.00119	
4.5	1280	0.00078	

( continued )

Table 5. NH<sub>3</sub> Data of Figure 28

Pressure (Micron)	Time Constant (Nano-sec)	Reciprocal Time Constant (Nano-sec <sup>-1</sup> )	Designation
70.0	390	0.00255	▲
59.5	400	0.00250	
50.0	410	0.00244	
39.5	450	0.00222	
32.5	500	0.00200	
25.5	600	0.00167	
20.0	650	0.00153	
15.0	700	0.00142	
11.0	850	0.00118	
7.5	950	0.00105	
4.5	1100	0.00091	

Table 6. Temperature Influence on Time Constant\*

Pressure (Micron)	Time Constant (Nano-sec)	Reciprocal Time Constant (Nano-sec <sup>-1</sup> )	Condition
89.4	327	0.00306	with dry ice
75.8	360	0.00278	
63.0	389	0.00257	
51.1	410	0.00244	
41.3	445	0.00225	
30.0	472	0.00212	
18.0	527	0.00190	
9.0	581	0.00172	
7.5	652	0.00153	

\* Both measurements were taken at same power level, 140 volts Stark voltage and with beat at 8.01 MHz.

( Continued )

Table 6. Temperature Influence on Time Constant\*

Pressure (Micron)	Time Constant (Nano-sec)	Reciprocal Time Constant (Nano-sec <sup>-1</sup> )	Condition
88.6	457	0.00219	without
69.9	480	0.00208	dry ice
50.2	525	0.00190	
27.5	623	0.00161	
16.7	681	0.00147	
11.7	775	0.00129	
8.0	842	0.00119	

\* Both measurements were taken at same power level, 140 volts Stark voltage and with beat at 8.01 MHz.

Table 7. Signal Amplitude and Temperature Relation

Pressure (Micron)	Signal Amplitude (Millivolt)	Temperature
107	8.8	dry ice temperature
71	11.4	
55	13.0	
37	14.4	
24	16.0	
13	17.6	
8	17.0	
2	15.4	
117	3.0	room temperature
69	3.7	
52	4.0	
33	4.2	
22	4.6	
14	4.7	
10	4.8	
9	4.7	

Table 8. Signal Amplitude and Klystron Power Relation

Klystron Power (Milliwatt)	Signal Amplitude (Millivolt)
0.60	7.0
0.64	8.6
0.80	9.9
0.84	10.8
1.18	12.0
1.60	13.2
1.72	13.5
2.00	14.0
2.50	14.4
3.12	14.2
3.70	13.7
4.22	12.8
4.90	11.0
6.00	8.5

## LITERATURE CITED

1. R. H. Dicke and R. H. Romer, Rev. Sci. Instr. 26, 915 (1955).
2. R. M. Hill, D. E. Kaplan, G. F. Herrmann, and S. K. Ichiki, Phys. Rev. Letter 18, 105 (1967).
3. F. Bloch, Phys. Rev. 70, 460 (1946).
4. R. H. Hughes and E. B. Wilson, Phys. Rev. 71, 562 (1947).
5. C. R. Nave, Ph.D. Thesis, Georgia Institute of Technology (1966).
6. W. Gordy, W. V. Smith and R. F. Trambarulo, Microwave Spectroscopy (Dover Publications, Inc., New York 1953), p. 192.
7. W. Gordy, W. V. Smith and R. F. Trambarulo, op cit., p. 194.
8. C. H. Townes, A. N. Holden and F. R. Merritt, Phys. Rev. 74, 1113 (1948).
9. H. Feeny, H. Lackner, P. Moser and W. V. Smith, J. Chem. Phys. 22, 79 (1954).
10. R. L. Legan, J. A. Roberts, E. A. Rinehart and C. C. Lin, J. Chem. Phys. 43, 4337 (1965).
11. W. Gordy, W. V. Smith and R. F. Trambarulo, op cit., p. 196.
12. P. W. Anderson, Phys. Rev. 75, 1450 (1949).
13. H. Margenau, Phys. Rev. 76, 1423 (1949).
14. C. M. Johnson and D. M. Slager, Phys. Rev. 87, 677 (1952).
15. R. Beringer and J. G. Castle, Jr., Phys. Rev. 81, 82 (1952).
16. R. M. Hill and W. Gordy, Phys. Rev. 82, 451 (1951).

17. B. Mäcke and P. Glorieux, Chem. Phys. Letters 14, 85 (1972).
18. R. M. Hill, D. E. Kaplan, G. F. Harman and S. K. Ichiki, op. cit., p.106.
19. W. Gordy, W. V. Smith and R. F. Trambarulo, op. cit., p. 193.
20. A. P. Cox, G. W. Flynn and E. B. Wilson, Jr. J. Chem. Phys. 42, 3094 (1965).
21. A. M. Ronn and E. B. Wilson, Jr. J. Chem. Phys. 46, 3262 (1967).

## VITA

The author, Foch Tsai, was born on april 3, 1939 in Shanghai, China. He received the B.S. degree from Chengkung University in 1960. He then served in the Army for a year and worked for the Chinese Petroleum Company for two years.

He came to the United States in 1963 and attended Northwestern State University in Louisiana, where he received the M.S. degree in mathematics in 1965. He continued his study at Louisiana State University in New Orleans and obtained his second M.S. degree in physics two years later. The author entered Georgia Institute of Technology in 1967 and currently is a candidate for Doctor of Philosophy degree in physics. He also serves as an instructor in the Physics Department, Morehouse College in Atlanta.